Journal of Molecular Structure 1321 (2025) 140197

Contents lists available at ScienceDirect

Journal of Molecular Structure

journal homepage: www.elsevier.com/locate/molstr

# Synthesis and biological studies of acetophenone-based novel chalcone, semicarbazone, thiosemicarbazone and indolone derivatives: Structure-Activity relationship, molecular docking, molecular dynamics, and kinetic studies

Aynur Farzaliyeva [a], Halil Şenol [b], Parham Taslimi [c,*], Furkan Çakır [b], Vagif Farzaliyev [d], Nastaran Sadeghian [c], Ibrahim Mamedov [a], Afsun Sujayev [d,*], Abel Maharramov [a], Saleh Alwasel [e], İlhami Gulçin [f]

[a] Faculty of Chemistry, Baku State University, Baku 1148, Azerbaijan
[b] Department of Pharmaceutical Chemistry, Faculty of Pharmacy, Bezmialem Vakif University, Fatih, Istanbul 34093, Türkiye
[c] Department of Biotechnology, Faculty of Science, Bartin University, Bartin 74110, Türkiye
[d] Laboratory of Physiologically Active Organic Compounds, Institute of Chemistry of Additives, Baku 1029, Azerbaijan
[e] Department of Zoology, King Saud University, College of Science, Riyadh 11362, Saudi Arabia
[f] Faculty of Science, Department of Chemistry, Atatürk University, Erzurum 25240, Türkiye

ARTICLE INFO

*Keywords:*
Chalcones
Thiosemicarbazones
Enzyme inhibition
Molecular docking
antioxidant activity

ABSTRACT

This study presents the synthesis and evaluation of nine acetophenone derivatives (**1–9**), with compounds **2, 4, 5, 6, 7,** and **9** being novel and synthesized for the first time. These derivatives encompass diverse structural motifs including chalcone, thiosemicarbazone, semicarbazone, and indolone derivatives. The structures of synthesized compound were confirmed by NMR analysis. The synthesized compounds were assessed for their in vitro enzyme inhibition against acetylcholinesterase (AChE), butyrylcholinesterase (BChE), and α-Glycosidase enzymes, as well as their antioxidant capacities using the DPPH radical scavenging assay. With Ki values ranging from 8.96±0.40 to 44.16±4.25 nM, these showed effective inhibition of AChE. However, the inhibitory characteristics of all drugs were almost the same. The Ki values of the two most active compounds, **(3)** and **(4)**, were 8.96±0.40 and 11.33±0.58 nM, respectively. Regarding α-Glycosidase, they demonstrate that all novel compounds **(1–9)** have $IC_{50}$ values between 30.16 and 133.98 μM, whereas the Ki values vary from 42.71±5.90 to 128.78±8.03 μM. Compound **4** emerged as a notable inhibitor, displaying significant inhibition against all used enzymes. Molecular docking studies revealed its exceptional binding affinities, corroborated by MM-GBSA ΔG binding free energies, and Glide Emodel scores. Compound **7** also exhibited promising inhibitory potential against α-Glycosidase. Docking scores for hAChE -12.207, for hBChE -10.140 and for α-Glycosidase -10.590 kcal/mol. The 250 ns molecular dynamics simulations confirmed the stability of the ligand-protein complexes, particularly with compound **4**. The ligand-protein complexes were found extremely stable according to the MD simulations. Additionally, ADME predictions indicated favorable pharmacokinetic properties and drug-likeness for all compounds, further supporting their potential as orally active agents. Compound **4**, in particular, stands out as a multitarget drug candidate, with strong inhibition against key enzymes implicated in neurodegenerative diseases and diabetes, suggesting its therapeutic potential in these conditions.

## 1. Introduction

Alzheimer's Disease (AD) is a progressive neurological disorder that leads to the degeneration and death of brain cells, causing memory loss, cognitive decline, and behavioral changes. It is the most common cause of dementia, a general term for conditions characterized by a severe decline in cognitive abilities that interfere with daily life [1–3]. The disease progresses through stages, starting from preclinical changes to

* Corresponding authors.
*E-mail addresses:* ptaslimi@bartin.edu.tr (P. Taslimi), s.afsun@mail.ru (A. Sujayev).

https://doi.org/10.1016/j.molstruc.2024.140197
Received 25 June 2024; Received in revised form 2 September 2024; Accepted 25 September 2024
Available online 26 September 2024
0022-2860/© 2024 Elsevier B.V. All rights are reserved, including those for text and data mining, AI training, and similar technologies.

mild, moderate, and severe AD, with increasing severity of symptoms. While the exact cause remains unclear, it involves a combination of genetic, lifestyle, and environmental factors, with age being a significant risk factor. Pathophysiologically, AD is characterized by amyloid-β plaques, neurofibrillary tangles, and loss of neuronal connections. Though there is no certain cure, treatments like cholinesterase inhibitors, memantine, lifestyle changes, and supportive care may help manage symptoms [4,5]. In AD, tAChE and BChE play significant roles in the disease's progression and treatment. Acetylcholine (ACh), a critical neurotransmitter for cognitive functions, is notably deficient in AD due to the degeneration of cholinergic neurons. AChE breaks down ACh in the synaptic cleft, and its inhibition is a primary treatment approach, as seen with medications like donepezil, rivastigmine, and galantamine, which increase ACh availability and improve cognitive function in early to moderate stages of AD. BChE also breaks down ACh, and its activity increases as AD progresses, further reducing ACh levels. Thus, targeting these enzymes to enhance ACh availability is a key strategy in managing AD's symptoms and slowing disease progression [6–8].

On the other hand, diabetes mellitus (DM) is a chronic metabolic disorder characterized by high blood sugar levels due to the body's inability to produce enough insulin, effectively use the insulin it produces, or both. There are two main types of Type-1 (T1DM) and Type-2 (T2DM) diabetes mellitus. Treatment of diabetes focuses on maintaining blood glucose levels within a target range to prevent complications. For T1DM, this requires regular insulin injections or an insulin pump. T2DM management often starts with lifestyle modifications, including a healthy diet, regular physical activity, weight loss, and oral medications that improve insulin sensitivity or reduce glucose production by the liver. α-Glycosidase (α-Gly) inhibition is an important therapeutic approach in managing diabetes, particularly T2DM. α-Gly is an enzyme in the small intestine that breaks down carbohydrates into glucose, leading to an increase in blood glucose levels post-meal. α-Gly inhibitors such as acarbose, miglitol, and voglibose, work by delaying the digestion and absorption of carbohydrates, which results in a slower and lower rise in blood glucose levels after meals [9–11].

Finally, antioxidant compounds are vital in metabolism as they neutralize free radicals and reactive oxygen species (ROS) and reduce oxidative stress, preventing cellular damage and supporting overall metabolic health. By stabilizing free radicals, antioxidants such as vitamins C and E, glutathione, and polyphenols protect lipids, proteins, and DNA, ensuring proper cellular function. They enhance the body's defense mechanisms, improve insulin sensitivity, and reduce inflammation, thereby helping to prevent and manage metabolic disorders like diabetes and cardiovascular diseases. Overall, antioxidants play a crucial role in maintaining metabolic balance and preventing related diseases [12–15].

Diabetes and AD share several common features, particularly in their pathophysiology and impact on the brain. Both conditions involve insulin resistance, with diabetes causing systemic insulin resistance and Alzheimer's disease involving brain insulin resistance, often termed "type 3 diabetes." Additionally, chronic inflammation and oxidative stress are central to both diseases, contributing to neuronal damage and cognitive decline in AD, and vascular complications in diabetes. Mitochondrial dysfunction and impaired glucose metabolism are also observed in both conditions, leading to energy deficits and further cellular damage. These shared mechanisms highlight the interconnected nature of metabolic and neurodegenerative disorders [16,17].

The chemistry of acetophenones is one of the most intensively developing areas of modern organic synthesis [18]. Chalcone, thiosemicarbazone, semicarbazone, indole, are important compounds in biology and medicine due to their diverse biological activities [19–24]. Chalcones exhibit antioxidant, anti-inflammatory, anticancer, and antimicrobial properties [25–29]. Thiosemicarbazones show antiviral, anticancer, and antibacterial effects. Semicarbazones are known for their anticonvulsant and antimicrobial properties [30]. Indole derivatives possess anticancer, neuroprotective, antimicrobial, and anti-inflammatory activities [31]. Pyrazoles exhibit anti-inflammatory, anticancer, analgesic, and antimicrobial effects [32]. Isoxazoles demonstrate antimicrobial, anti-inflammatory, anticancer, and analgesic properties [33,34].

The aim of this study was to synthesize new chalcone, thiosemicarbazone, semicarbazone and indolone based on substituted acetophenones and to investigate their biological activities. For this purpose, a total of nine compounds were synthesized and in vitro enzyme inhibition studies of all compounds were performed against human AChE, human BChE and α-Glycosidase enzymes. Additionally, the DPPH radical scavenging effects of all compounds were investigated and their antioxidant capacities were determined. In addition, molecular docking and molecular dynamics studies were carried out in order to evaluate the inhibition mechanisms and to determine the stability of the ligand-protein complexes of the most active compounds. Finally, in silico ADME (Absorption, Distribution, Metabolism, and Excretion) properties of all the synthesized compounds were carried out and drug likeness were discussed.

## 2. Results and discussion

### 2.1. Organic synthesis

In this study a total of nine representatives of the acetophenone derivatives **(1–9)** were synthesized. Compounds **2, 4, 5, 6, 7, and 9** were synthesized for the first time in this study, but **1, 3** and **8** are known in literature [35–37]. Compounds **1–3** are chalcone derivatives, compounds **4–6** are thiosemicarbazone derivatives, compound **7** is semicarbazone derivative and finally compounds **8** and **9** are indolone derivatives. The chemical formulas of the target compounds are given in Fig. 1**.** In addition, the synthetic steps of all the synthesized compounds are given in Schemes 1–4.

#### 2.1.1. Synthesis of chalcone derivatives (1–3)

The synthesis of chalcones was carried out by Claisen-Schmidt condensation. Starting from corresponding benzaldehyde and acetophenone derivatives the chalcone compounds **(1–3)** were synthesized in the presence of catalytic amounts of piperidine in ethanol at room temperature (Scheme 1).

#### 2.1.2. Synthesis of semi- and thiosemicarbazone derivatives (4–7)

For the synthesis of the compound **4** initially corresponding chalcone **(A)** was synthesized from the reaction of 5-brormosalycilaldehyde and 2-methyl-4-hydroxy-acetophenone. Then the chalcone (**4**) was reacted with thiosemicarbazide in dimethylsulfoxide (DMSO) at high temperature and compound **4** was obtained (Scheme 2).

On the other hand, for the synthesis of compounds **5–7** corresponding acetophenone derivatives reacted with semicarbazide or thiosemicarbazide in DMSO at high temperature. As conclusion compound **5** and **6** were obtained from reaction with thiosemicarbazide, compound 7 was obtained from reaction with semicarbazide (Scheme 3).

#### 2.1.3. Synthesis of indolone derivatives (8–9)

For the synthesis of the indolone derivatives **(8 and 9)** the corresponding acetophenone derivatives were reacted with isatin (Scheme 4).

The chemical structure of all the synthesized compounds were confirmed by $^{1}H$ and $^{13}C$ Nuclear Magnetic Resonance (NMR) analyses.

### 2.3. In vitro biological activity studies

The in vitro enzyme inhibition studies of all compounds were performed against AChE, human BChE and α-Glycosidase enzymes. Additionally, the DPPH radical scavenging effects of all compounds were investigated, and their antioxidant capacities were determined. The results are given in Table 1**.**

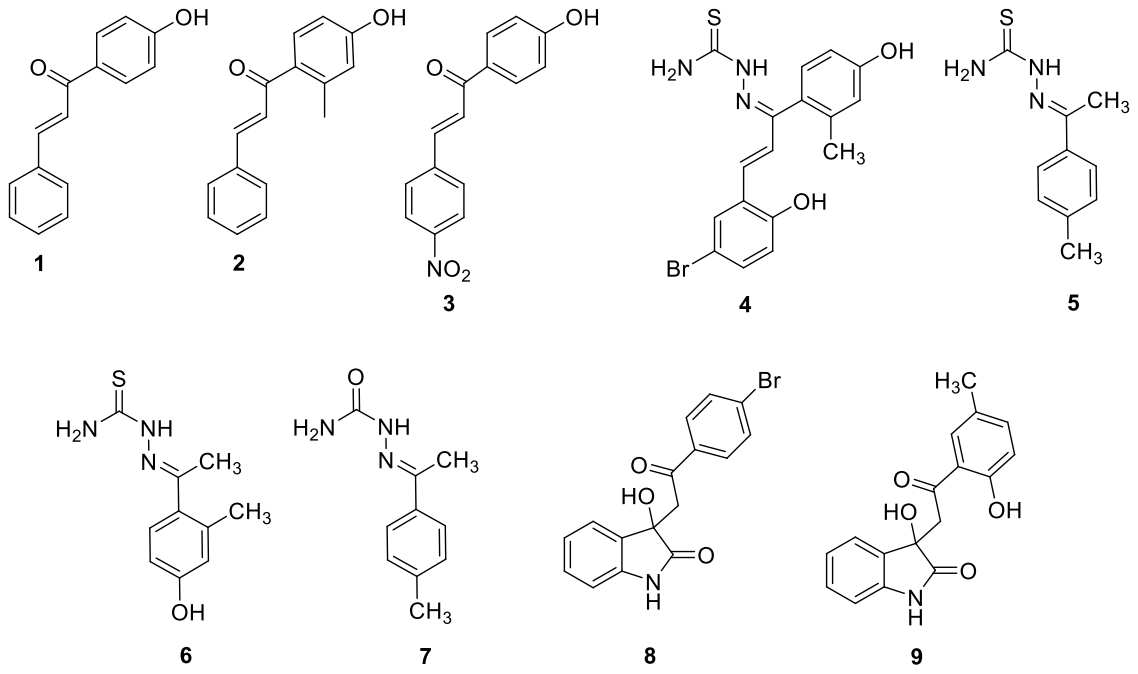


**Fig. 1.** Chemical structures of compounds **1–9**.

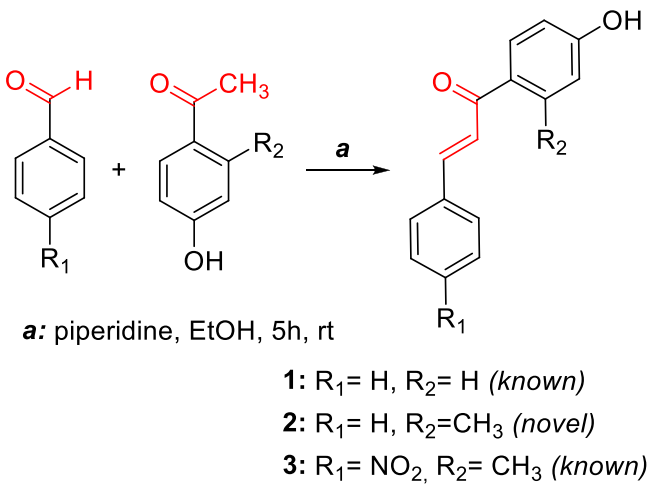


**Scheme 1.** Synthesis of chalcone derivatives **(1–3)**.

*2.3.1. AChE and BCHE inhibition results*

All of the new compounds (**1–9**) exhibited much more AChE inhibitory action than Tacrine (TAC), the traditional AChE inhibitor. An overview of the Ki values for the generated compounds and standard chemical is given in Table 1. These demonstrated efficient inhibition of AChE, with $K_i$ values ranging from 8.96±0.40 to 44.16±4.25 nM. All of these substances did, however, have nearly identical inhibitory profiles. 8.96±0.40 and 11.33±0.58 nM were the $K_i$ values of the two most active compounds (**4**) and (**3**), respectively. The following is the order of the $IC_{50}$ values for the active substances and the positive control: **4** (10.53 nM, $r^2$: 0.942) < **3** (14.24 nM, $r^2$: 0.925) < **8** (18.71 nM, $r^2$: 0.928) < **9** (21.93 nM, $r^2$: 0.951) < **7** (39.35 nM, $r^2$: 0.925) < **5** (41.66 nM, $r^2$: 0.925) < TAC (305.87 nM, $r^2$: 0.984). When we looked at the data, we found that the compound (**2**) for this enzyme ($IC_{50}$: 58.04 nM) was weak when compared to the values of other substances, but the standard value ($IC_{50}$: 305.87 nM) produced good results. The middle inhibitor for this enzyme was found to be compound (**7**), as the findings stay good until the compound starts to increase ($IC_{50}$: 39.35 nM). Also, compared to TAC, all of the new compounds (**1–9**) demonstrated noticeably stronger BChE inhibitory actions. With $K_i$ values of 1.42 and 4.12 nM, compounds (**3**) and (**4**) are likewise the most active for BChE, much as AChE. Reducing the cytotoxicity has the potential to decrease the amount of

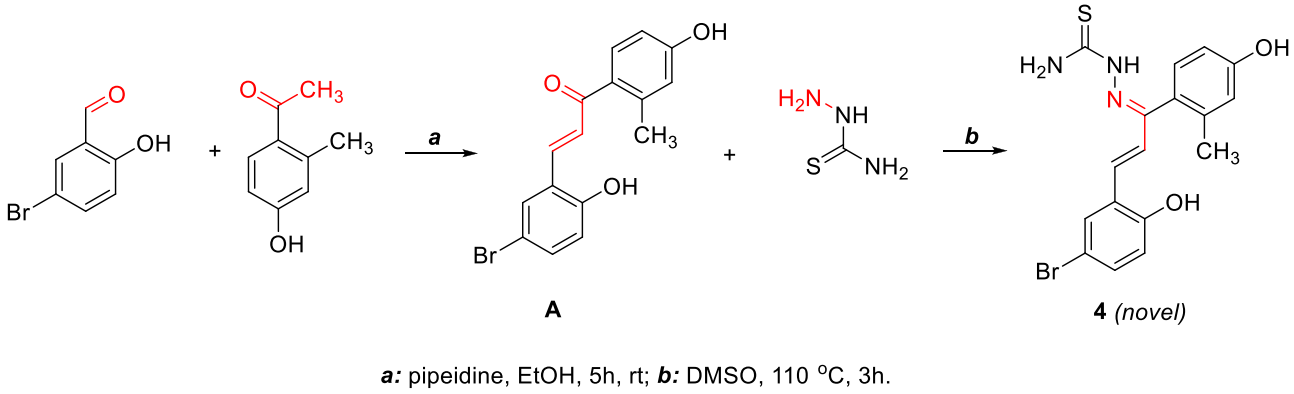


**Scheme 2.** Synthesis of compound 4.

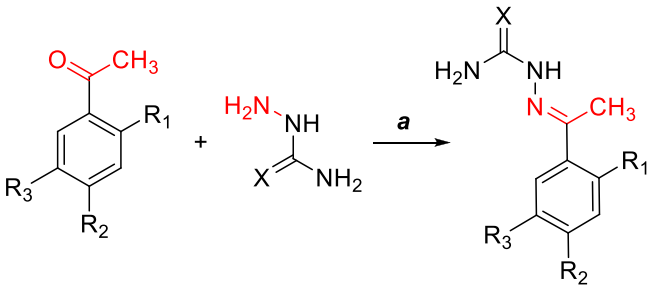


**5:** $R_1$= H, $R_2$= $CH_3$, $R_3$= H, X= S
**6:** $R_1$= OH, $R_2$= H, $R_3$= $CH_3$, X= S
**7:** $R_1$= H, $R_2$= $CH_3$, $R_3$= H, X= O

**Scheme 3.** Synthesis of compound 5–7.

fibrous amyloid-β protein in cortical structures, as demonstrated by BChE and mice kinetic models. The amino acid sequences of AChE and BChE are 54 % similar, and the active sites are situated at the base of a 20 Å deep canyon [36]. These two enzymes' catalytic triad, acyl binding pockets, and choline binding sites make up their active sites. BChE inhibitors offer a lot of promise for treating AD since they can avoid the cholinergic toxicity of AChE inhibitors. The primary treatment for AD at the moment is cholinergic medications; but, because the human brain is complex, there are other targets and pathways that can control how quickly AD progresses [37]. For BChE, the following is the order of the $IC_{50}$ values for the active substances and the positive control: **3** (1.42 nM, $r^2$: 0.963) < **4** (4.12 nM, $r^2$: 0.902) < **8** (5.48 nM, $r^2$: 0.966) < **9** (7.96 nM, $r^2$: 0.930) < **6** (16.92 nM, $r^2$: 0.952) < TAC (72.71 nM, $r^2$: 0.975).

### 2.3.2. α-Glycosidase inhibition results

Table 1 shows that the $IC_{50}$ values of all the new compounds (**1–9**) for enzyme α-Glycosidase range from 30.16 to 133.98 μM, whereas the $K_i$ values fall between 42.71±5.90–128.78±8.03 μM. The findings unambiguously demonstrate that every one of the novel compounds (**1–9**) exhibited α-Glycosidase's inhibitory actions in a manner comparable to Acarbose ($IC_{50}$: 575.02 μM), a common glycosidase inhibitor. The $K_i$ values of **7, 8, 9**, and **4** that were found to be the most effective were 42.71±5.90, 67.56±3.87, 71.80±6.81, and 76.54±6.74 μM, respectively. The following is a list of the most active compounds, arranged with ACR serving as the positive control: **7** (30.16 μM, $r^2$: 0.931) < **8** (56.28 μM, $r^2$: 0.927) < **9** (65.21 μM, $r^2$: 0.946) < **4** (69.57 μM, $r^2$: 0.935) < **1** (101.25 μM, $r^2$: 0.998) < **5** (112.01 μM, $r^2$: 0.956) < Acarbose (575.02 μM, $r^2$: 0.979). Based on these data, compounds **7** and **4** are the most potent α-Glycosidase inhibitors, with potencies about 8 and 14 times higher than that of the conventional inhibitor Acarbose, respectively. Furthermore, although having the lowest inhibition in the entire series, compound **3** is only **4** times as effective as Acarbose. α-Glycosidase inhibitors have the ability to postpone the breakdown of carbohydrates in the small intestine, which consequently lowers postprandial blood glucose levels [38]. Acarbose, voglibose, and miglitol are among the α-glycosidase inhibitors that are now being used as therapeutic medications to treat T2DM. However, due to side effects including

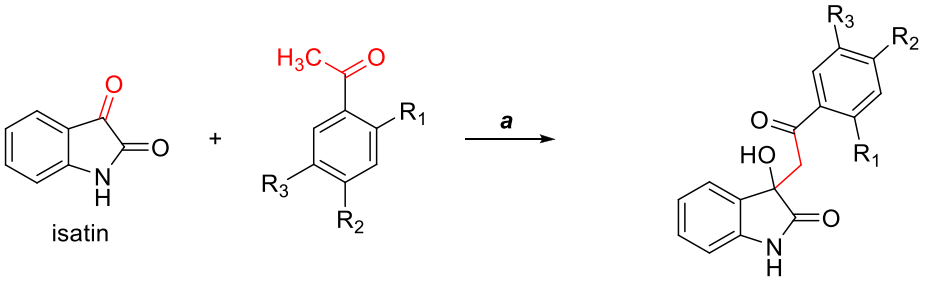


**8:** $R_1$= H, $R_2$= Br, $R_3$= H *(knwon)*
**9:** $R_1$= OH, $R_2$= H, $R_3$=$CH_3$ *(novel)*

**Scheme 4.** Synthesis of compound 8 and 9.

**Table 1**
The enzyme inhibition results of the synthesized compounds (**1–9**) against α-Gly, AChE and BChE enzymes as well as DPPH radical scavenging activity.

| Cpds. | $IC_{50}$ | | | | Ki (nM) | | |
|---|---|---|---|---|---|---|---|
| | DPPH (μg/mL) | AChE (nM) | BChE (nM) | α-Gly (μM) | AChE (nM) | BChE (nM) | α-Gly (μM) |
| **1** | 18.06 | 46.22 | 20.75 | 101.25 | 38.53±2.44 | 15.91±1.34 | 122.18±16.05 |
| **2** | 22.53 | 58.04 | 25.42 | 125.53 | 44.16±4.25 | 21.83±2.38 | 127.58±11.34 |
| **3** | 22.01 | 14.24 | 1.42 | 133.98 | 11.33±0.58 | 0.94±0.08 | 156.61±9.76 |
| **4** | **16.85** | **10.53** | **4.12** | **69.57** | **8.96±0.40** | **3.63±0.21** | **76.54±6.74** |
| **5** | 77.51 | 41.66 | 21.67 | 112.01 | 36.12±3.25 | 19.72±2.34 | 119.93±9.31 |
| **6** | 62.08 | 48.19 | 16.92 | 116.45 | 40.52±4.38 | 16.14±1.48 | 128.78±8.03 |
| **7** | 14.74 | 39.35 | 23.96 | **30.16** | **32.95±3.91** | **20.52±3.50** | **42.71±5.90** |
| **8** | 40.07 | 18.71 | 5.48 | 56.28 | 16.86±1.53 | 4.21±0.41 | 67.56±3.87 |
| **9** | 28.55 | 21.93 | 7.96 | 65.21 | 18.31±1.32 | 5.62±0.35 | 71.80±6.81 |
| **Tac**[a] | – | 305.87 | 72.71 | – | 254.87±16.97 | 64.18±5.98 | – |
| **Riv**[a] | – | 2290.97 | 105.30 | – | – | – | – |
| **Acr**[a] | – | – | – | 575.02 | – | – | 603.68±28.03 |
| **Tro**[a] | 9.75 | – | – | – | – | – | – |

[a] **Tac** = Tacrine and **Riv** = Rivastigmine were used as reference inhibitors for ChEs inhibition; **Acr** = Acarbose was used as reference inhibitor for α-Glycosidase and **Tro** = Trolox was used as a reference inhibitor for DPPH radical scavenging assay.

diarrhea and flatulence, these clinical medications also have significant restrictions. Therefore, the development of safe and effective α-glycosidase inhibitors is required for the management of T2DM [38,39].

### 2.3.3. Enzyme kinetics and mode of inhibition

Kinetic analyses for the potent inhibitor **4d** were performed using BChE and AChE to characterize the cholinesterase inhibitory properties of several novel compounds. Compound **4** was the most potent inhibitor, showing the lowest $IC_{50}$ values (4.12 nM) against BChE and (10.53 nM) against AChE. The compound was produced at doses of $IC_{50}/3$, $IC_{50}$, and $3 \times IC_{50}$. Lineweaver-Burk plots can be used to distinguish between subtypes of reversible inhibition, such as competitive, uncompetitive, noncompetitive, and mixed forms of inhibition. Lineweaver–Burk graphics have demonstrated that uncompetitive inhibition can be detected when the lines are parallel to one another. The studied compounds shown to have an uncompetitive type manner of inhibition for α-glycosidase upon closer inspection. Since the inhibitors only bind to the enzyme target when both the substrate and the target are present and the enzyme is active, this mechanism of action is very appealing for drug design. Conversely, uncompetitive inhibitors exhibit increased inhibition with increasing substrate and decrease substrate $K_m$ and $V_{max}$. As a result, unlike irreversible enzyme inhibitors, the explored candidate has uncompetitive type forces, which has led to investigations on enzyme kinetics demonstrating its biological significance. In this study, after studying AChE and BChE enzymes, $K_i$ graphs were obtained with competition, the results on this α-glycosidase enzyme were determined noncompetition.

### 2.3.4. DPPH radical scavenging activity results

The deep purple DPPH radical test is one of the few persistent organic nitrogen radicals. The reducing ability of antioxidant chemicals toward DPPH radicals is measured, and this is the basis for this process. Table 1 displays $IC_{50}$ of the compounds under investigation in comparison to a reference radical scavenger such as Trolox. The investigated chemicals' $IC_{50}$ values were determined to be 14.74 μg/mL for compound **7**, 16.85 μg/mL for compound **4**, 9.36 mg/mL for α-Tocopherol, 10.66 mg/mL for Trolox, and 17.77 mg/mL. In small doses, antioxidants can prevent DNA mutations, malignant changes, oxidative stress, and various forms of cell damage. They can also delay or stop the oxidation of proteins, carbohydrates, lipids, and nucleic acids, which are examples of biomolecules. Spectrophotometry is commonly used to determine a substance's antioxidant capability by quantifying its capacity to scavenge DPPH radicals. The most popular technique for quickly assessing an organic compound's capacity to scavenge free radicals is the DPPH radical model. Highly reactive substances are known as ROS, which also include hydrogen peroxide ($H_2O_2$), hydroxyl radicals (·OH), superoxide anion radicals, and singlet oxygen ($^1O_2$). These radicals can all generate more ROS [40]. ROS have a number of detrimental effects and can cause cancer, atherosclerosis, diabetes, and ischemic heart disease, among other disorders. Furthermore, food quality deterioration, which causes toxicity, rancidity, and the loss of essential biochemical components in physiologic metabolism, is associated with ROS. Thus, developing effective, low-risk antioxidant reagents is essential to eliminating free radicals from the human body [41]. Additionally, when we compared it to Trolox, the results of some compounds were similar (Compounds **7** and **4**) and some were 3–8 times weaker (Compounds **9, 8, 6** and **5**).

## 2.4. Molecular docking studies

Molecular docking is a key computational technique in drug discovery, predicting how potential drugs bind to target proteins. It helps identify promising candidates, optimize their structures, understand their mechanisms, and even repurpose existing drugs for new uses. This accelerates drug development by guiding the design of effective medications for various diseases [40].

In molecular docking, IFD (Induced Fit Docking), MMGBSA (Molecular Mechanics Generalized Born Surface Area), and Glide Emodel are essential models used to predict and evaluate ligand-receptor interactions and binding modes. IFD accommodates protein flexibility by refining the receptor's active site and optimizing the ligand's conformation for a better fit, thereby enhancing accuracy in predicting binding affinity. MMGBSA calculates the binding free energy of ligand-receptor complexes, considering both enthalpic and entropic contributions, providing a comprehensive assessment of binding affinity [41,42].

In this study to evaluate the prospective inhibition mechanism, molecular mechanics and determine the binging modes via ligand-protein interactions, molecular docking studies were carried out against hAChE, hBChE and α-Glycosidase enzymes. The IFD extra precision (XP) Glide Scores (Gscores), MM-GBSA ΔG binding free energies and glide emodel scores of the synthesized compounds are given in Table 2.

As can be seen from Table 2, compound **4** has the best docking score against all three enzyme types. The docking scores of compound **4** against hAChE, hBChE and α-Gly were found to be −12.207, −10.140 and −10.590 kcal/mol, respectively. Compound **4** is also the compound with the best $IC_{50}$ value as the best inhibitor candidate against hAChE and hBChE in in vitro tests. Although the $IC_{50}$ value of compound **7** against the α-Glycosidase enzyme is better than the $IC_{50}$ value of compound **4**, molecular docking studies revealed the potential of compound **4** to be an inhibitor of α-Glycosidase. The docking score of compound **7** against α-Glycosidase enzyme was found to be 8.016 kcal/mol.

The docking scores of other compounds against the hAChE enzyme range from −7.660 to −10.773 kcal/mol, against hBChE from −6.773 to −9.146 kcal/mol, and against the α-Glycosidase enzyme from −7.034 to −8.452 kcal/mol. Evaluating the MM-GBSA ΔG free binding energies, compound **4**′s scores are −79.03 kcal/mol for hAChE, −48.36 kcal/mol for hBChE, and −67.91 kcal/mol for α-Glycosidase, the best among all compounds for each respective enzyme. These scores highlight the potential of compound **4** as a strong inhibitor candidate. Although compound **7** is the most active in vitro against the α-Glycosidase enzyme, its MM-GBSA score is not superior to compound **4**, indicating the need for further MD simulations of compound **4**. Additionally, compound **4** excels with the best Glide Emodel scores for all three enzyme types, further distinguishing it from the other compounds. According to the results obtained from Table 2, two-dimensional (2D) and three-dimensional (3D) ligand-protein interactions of compound **4** in all three enzyme types were examined and the results were evaluated.

### 2.4.1. Molecular docking analysis on hAChE

The 2D and 3D ligand-protein interactions between compound **4** and hAChE are given in Fig. 2. Also, Fig. 2**a** represent the 2D ligand-protein interactions of **4-hAChE** complex. As seen in Fig. 2a, the amino group of thiosemicarbazone moiety formed two different hydrogen bond interactions (purple arrows) with Tyr-72 and His-287. In addition, the phenolic hydroxyl groups also formed three different hydrogen bond interactions with Val-73, Asp-74 and Thr-75. The brominated phenyl ring formed a π-π stacking interaction (green line) with Tyr-341 and bromine atom formed a halogen bond interaction (brown arrow) with Phe-295.

Fig. 2**b** represents the 3D ligand-protein interactions of **4-hAChE** complex. In Fig. 2**b**, the yellow dashes indicate the hydrogen bond interactions, the turquoise dashes indicate the π-π stacking interaction and the purple dashes represents the halogen bond interactions. The hydrogen bond lengths vary from 1.71 to 2.21 Å. The shorter bonds represent the more stable complexes [43,44]. On the other hand, the while the length of halogen bond was measured as 2.45 Å the length of π-π stacking interaction is 3.50 Å. While in Fig. 2**a**, there is only one hydrogen bond interaction between Thr-75 and the phenolic hydroxyl, in Fig. 2**b**, both the carbonyl and amino group of Thr-75 make hydrogen bonds with phenolic hydroxyl. A total of six hydrogen bonds contribute to the formation of a stable complex.

**Table 2**
Docking scores, MM-GBSA ΔG binding free energies and glide emodel scores of the synthesized compounds.

| | IFD XP GScores (kcal/mol) | | | MM-GBSA ΔG Bind. (kcal/mol) | | | Glide Emodel (kcal/mol) | | |
|---|---|---|---|---|---|---|---|---|---|
| Cpds. | hAChE 4M0E | hBChE 5NN0 | α-Gly 3WY1 | hAChE 4M0E | hBChE 5NN0 | α-Gly 3WY1 | hAChE 4M0E | hBChE 5NN0 | α-Gly 3WY1 |
| **1** | −10.428 | −9.146 | −8.044 | −60.76 | −45.31 | −49.08 | −60.526 | −56.954 | −55.341 |
| **2** | −10.773 | −8.528 | −8.452 | −58.23 | −50.58 | −59.01 | −63.152 | −57.270 | −63.019 |
| **3** | −10.595 | −7.603 | −8.344 | −55.95 | −44.84 | −61.43 | −66.492 | −62.447 | −79.890 |
| **4** | **−12.207** | **−10.140** | **−10.590** | **−79.03** | **−48.36** | **−67.91** | **−88.816** | **−81.648** | **−84.188** |
| **5** | −7.660 | −8.515 | −7.514 | −57.13 | −33.29 | −25.94 | −65.466 | −47.152 | −47.176 |
| **6** | −7.813 | −8.059 | −8.011 | −47.81 | −30.15 | −39.77 | −53.431 | −45.572 | −47.634 |
| **7** | −9.876 | −6.991 | **−8.016** | −30.68 | −37.74 | **−44.60** | −60.541 | −54.773 | **−60.353** |
| **8** | −8.329 | −6.773 | −7.034 | −55.38 | −39.39 | −56.77 | −71.114 | −57.212 | −64.452 |
| **9** | −9.758 | −7.310 | −7.188 | −63.28 | −54.08 | −64.43 | −67.285 | −54.928 | −71.835 |

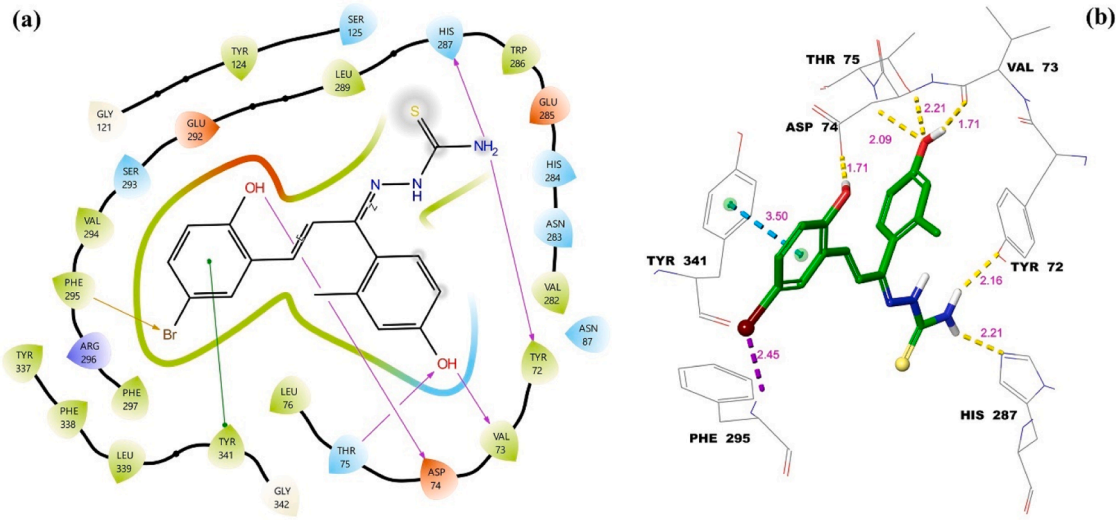


**Fig. 2.** The 2D (a) and 3D (b) ligand-protein interactions between compound **4** and hAChE.

*2.4.2. Molecular docking analysis on hBChE*

The 2D and 3D ligand-protein interactions between compound **4** and hBChE are given in Fig. 3. Fig. 3**a** represent the 2D ligand-protein interactions of **4-hBChE** complex. As seen in Fig. 3**a,** the thiocarbonyl and amino groups atom of thiosemicarbazone moiety formed two different hydrogen bond interactions with Thr-120 and Asn-83, respectively. The phenolic hydroxyl groups of both phenyl rings also formed two additional hydrogen bond interaction with Pro-285 and His-438. Finally, brominated phenyl ring formed π-π stacking interaction.

Fig. 3**b** represent the 3D ligand-protein interactions of **4-hBChE** complex. In Fig. 2**b,** the yellow dashes indicate the hydrogen bond interactions and the turquoise dashes indicate the π-π stacking interactions. The lengths of the hydrogen bond vary from 1.95 to 2.69 Å. As can be seen from Fig. 3**b,** two phenyl rings are positioned perpendicular to each other. The fact that the thiosemicarbazone group makes two hydrogen bonds is very important in terms of inhibition and complex stability.

*2.4.3. Molecular docking analysis on α-glycosidase*

The 2D and 3D ligand-protein interactions between compound **4** and

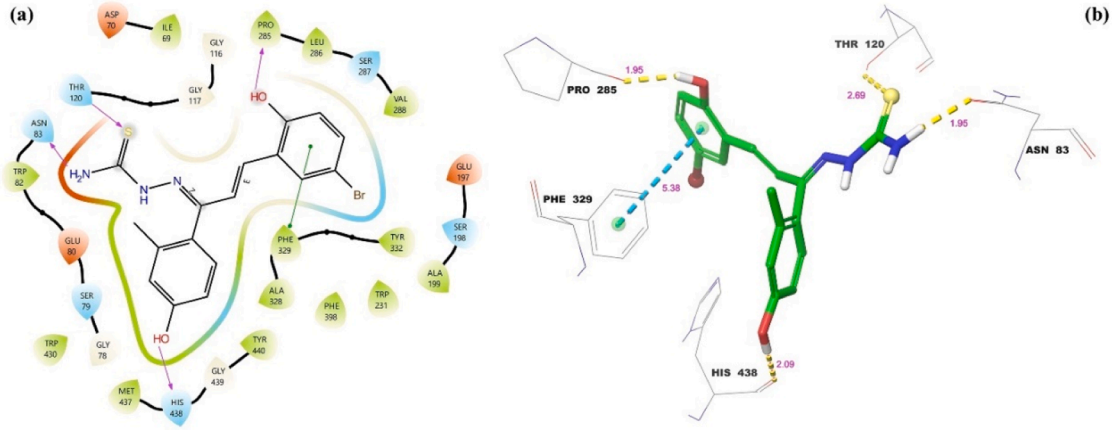


**Fig. 3.** The 2D (a) and 3D (b) ligand-protein interactions between compound **4** and hBChE.

α-Glycosidase are given in Fig. 4. Fig. 4**a** represent the 2D ligand-protein interactions of **4-α-Glycosidase** complex. As seen in Fig. 4**a,** there are four different hydrogen bond interactions between compound **4** and the active site of the α-glycosidase enzyme. The amino groups of thiosemicarbazide moiety formed two different hydrogen bond interactions with Gly-228. In addition, the hydroxyl groups of both phenyl rings formed also two hydrogen bond interactions with Hie-332 and Tyr-235. Both phenyl ring formed aa π-π stacking interaction with Tyr-65 and Phe-297. Finally, the brominated phenyl ring formed a π-cationic bond interaction with Arg-400.

Fig. 4**b** represent the 3D ligand-protein interactions of **4-α-Glycosidase** complex. In Fig. 4**b,** the yellow dashes indicate the hydrogen bond interactions, the turquoise dashes indicate the π-π stacking interaction, the purple dashes represent the halogen bond interaction and the red dashes represents the π-cationic bond interaction. The lengths of hydrogen bonds vary from 1.83 to 2.17 Å. As can be seen in Fig. 4**b**, the brominated phenyl ring interacted with multiple amino acid residues and formed a stable binding mode. On the other hand, the thiosemicarbazone group created a unique binding mode with two different hydrogen bond interactions.

As conclusion of molecular docking studies compound **4** demonstrated significant interactions with hAChE, hBChE, and α-Glycosidase enzymes, indicating its potential as a robust inhibitor candidate. For hAChE, compound **4** formed critical hydrogen bonds with Tyr-72, His-287, Val-73, Asp-74, and Thr-75, as well as π-π stacking with Tyr-341 and halogen bond with Phe-295, contributing to a stable complex with a total of six hydrogen bonds. In hBChE, compound **4** displayed vital hydrogen bonds with Thr-120 and Asn-83, and additional interactions with Pro-285 and His-438, along with π-π stacking interactions, reinforcing complex stability. For α-Glycosidase, compound **4** formed four hydrogen bonds with Gly-228, Hie-332, and Tyr-235, π-π stacking interactions with Tyr-65 and Phe-297, and a π-cationic bond with Arg-400, resulting in a highly stable binding mode. These interactions, characterized by extensive hydrogen bonding, π-π stacking, and halogen bonding, highlight compound **4**′s strong binding affinities and its potential as a highly effective inhibitor for these enzymes.

### 2.5. Molecular dynamics (MD) simulations

Molecular dynamics (MD) simulations are crucial in drug design, providing atomic-level insights into the dynamic behavior of molecules. In addition, MD help identify drug targets, optimize lead drugs, and understand binding affinities and stability of ligand-protein complexes [45,46]. In this study MD simulations were carried out to evaluate the stabilities of the ligand-protein complexes and also to determine key interactions between ligands and proteins. 250 nanosecond MD simulations were carried out for 4-hAChE, 4-hBChE and 4-α-Glycosidase ligand protein complexes.

#### 2.5.1. MD simulation analysis of 4-hAChE complex

Compound **4** was found to be the most active compounds in vitro and *in silico* tests against hAChE. The 250 ns MD simulation analysis of **4-hAChE** complex is given in Fig. 5. Fig. 5**a** represents the 2D key ligand-protein interactions during simulation time. As seen in Fig. 5**a,** the amino group of thiosemicarbazone moiety formed a hydrogen bond interaction (purple arrow) with Glu-292 (44 % of the simulation time) and the sulfur atom of same group formed another hydrogen bond interaction with Ser-293 (30 % of the sim.). On the other hand, phenolic hydroxyl of brominated ring formed a direct hydrogen bond interaction (39 % of the sim.) and two water-bridged hydrogen bond interaction (22 and 23 % of the sim.) with Asp-74. Finally, brominated phenyl ring also formed a π-π stacking interaction (yellow line) with Tyr-341 (30 % of the sim.).

Fig. 5**b** represents the RMSD (root mean square deviation) values of protein and ligand atoms. While the average RMSD of protein Cα atoms was calculated as 2.5 Å (pale blue), the average RMSD of ligand atoms was calculated as 5.31 Å (red). The average deviation of the ligand from its original position was calculated as 0.6 Å (pink). While the deviation of 2.5 Å for the protein backbone is normal, the deviation of 5.31 Å for the ligand atoms is a bit high, but the ligand and protein remained stable during the simulation time. Figs. 5**c** and 5**d** represent the RMSF (root mean square fluctuation) of protein Cα atoms and ligand atoms, respectively. In Fig. 5**c** the green vertical lines indicate the ligand-protein contacts. The average RMSF of protein Cα atoms was calculated as 1.2 Å. on the other hand, the average RMSF of the ligand atoms was calculated as 1.5 Å. These small fluctuations in the protein and ligand atoms indicate that the complex is extremely stable throughout the simulation time. Fig. 5**e** shows a fractional interaction histogram over simulation time, where amino acids can interact with multiple functional groups simultaneously. A value of 0.8 means an amino acid interacts for 80 % of the time, while values over 1.0 indicate interactions with multiple parts exceeding 100 %. Blue indicates water-bridged hydrogen bonds, green indicates hydrogen bonds, and purple indicates hydrophobic interactions. According to the Fig. 5**e,** the most abundant interactions involve Trp-286, Asp-74, Glu-292, and Ser-293, which are key for inhibition. These four amino acid residues are the key amino acid residues for inhibition.

#### 2.5.2. MD simulation analysis of 4-hBChE complex

Compound **4** was also found to be the most active compounds as in vitro and *in silico* tests against hBChE. The 250 ns MD simulation analysis of **4-hBChE** complex is given in Fig. 6. Fig. 6**a** represents the 2D key

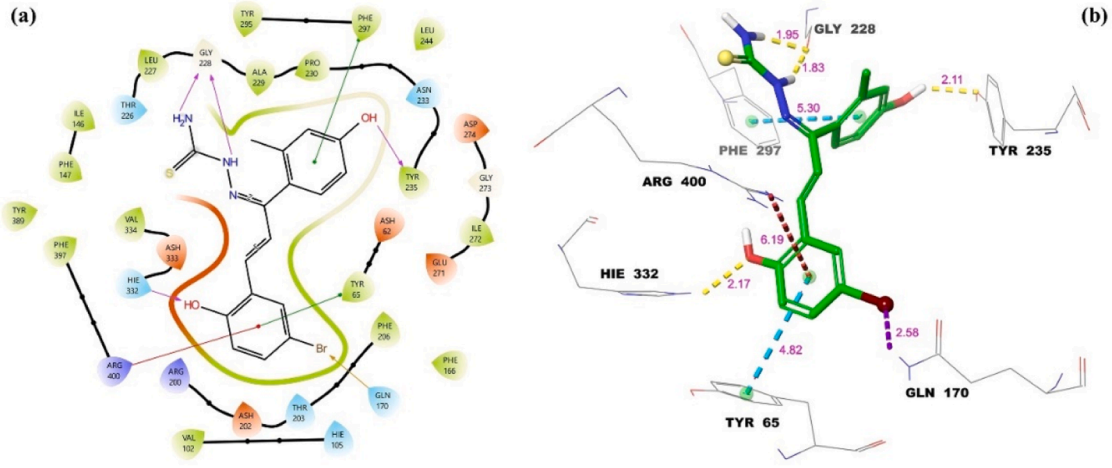


**Fig. 4.** The 2D (a) and 3D (b) ligand-protein interactions between compound **4** and α-Gly.

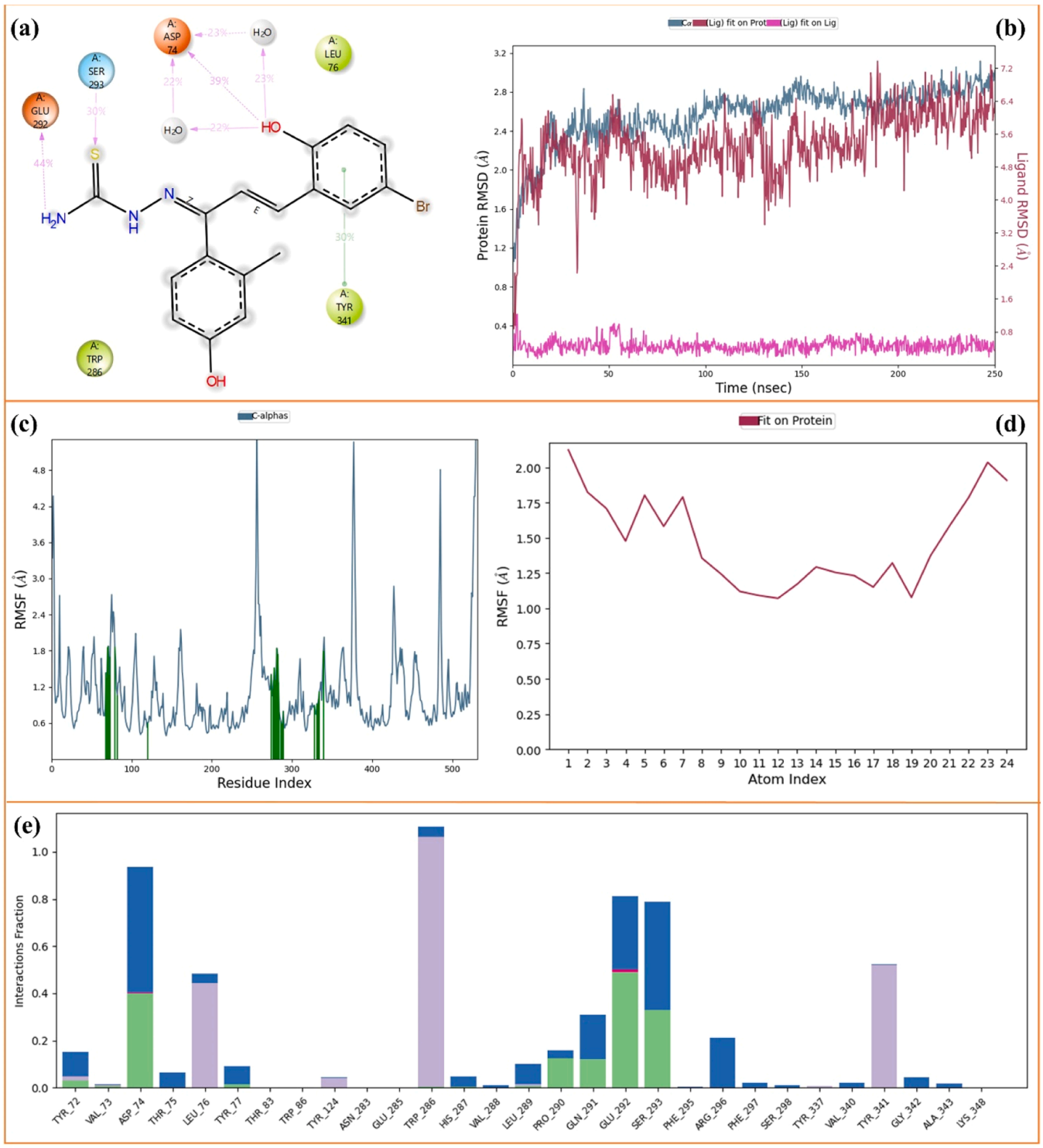


**Fig. 5.** The 250 ns MD simulation analysis of **4-hAChE** complex. (a) 2D key interactions, (b) RMSD values of ligand and protein, (c) RMSF values of protein Cα atoms, (d) RMSF values of ligand atoms, (e) fractional interaction histogram.

ligand-protein interactions during simulation time. As seen in Fig. 6**a,** the hydroxyl group of the brominated phenyl ring formed a hydrogen bond with Ser-287 (22 % of the sim.) and Leu-286 (29 % of the sim.). In addition, other phenolic hydroxyl group also formed a hydrogen bon interaction with Thr-120 (20 % of the sim.). While the amino group of thiosemicarbazone moiety formed a water-bridged hydrogen bond interaction with Glu-276 (23 % of the sim.) the brominated phenyl ring formed a π-π stacking interaction with Phe-329 (28 % of the sim.). Fig. 6**b** represents the RMSD values of protein and ligand atoms. The average RMSD of protein Cα atoms was calculated as 2.3 Å (pale blue). The average RMSD value of ligand atoms was calculated as 4 Å. While the RMSD value of the ligand atoms was 1.5 Å on average in the first 75 ns of the simulation, after this stage, the complex moved its final form and the RMSD value increased to 4.5 Å, but it remained stably bound to the protein until the end of the simulation. The average deviation of ligand from its original position was calculated as 0.8 Å (pink).

Figs. 6**c** and 6**d** indicate the RMSF values of protein Cα atoms and ligand atoms, respectively. the average RMSF of protein Cα and ligand

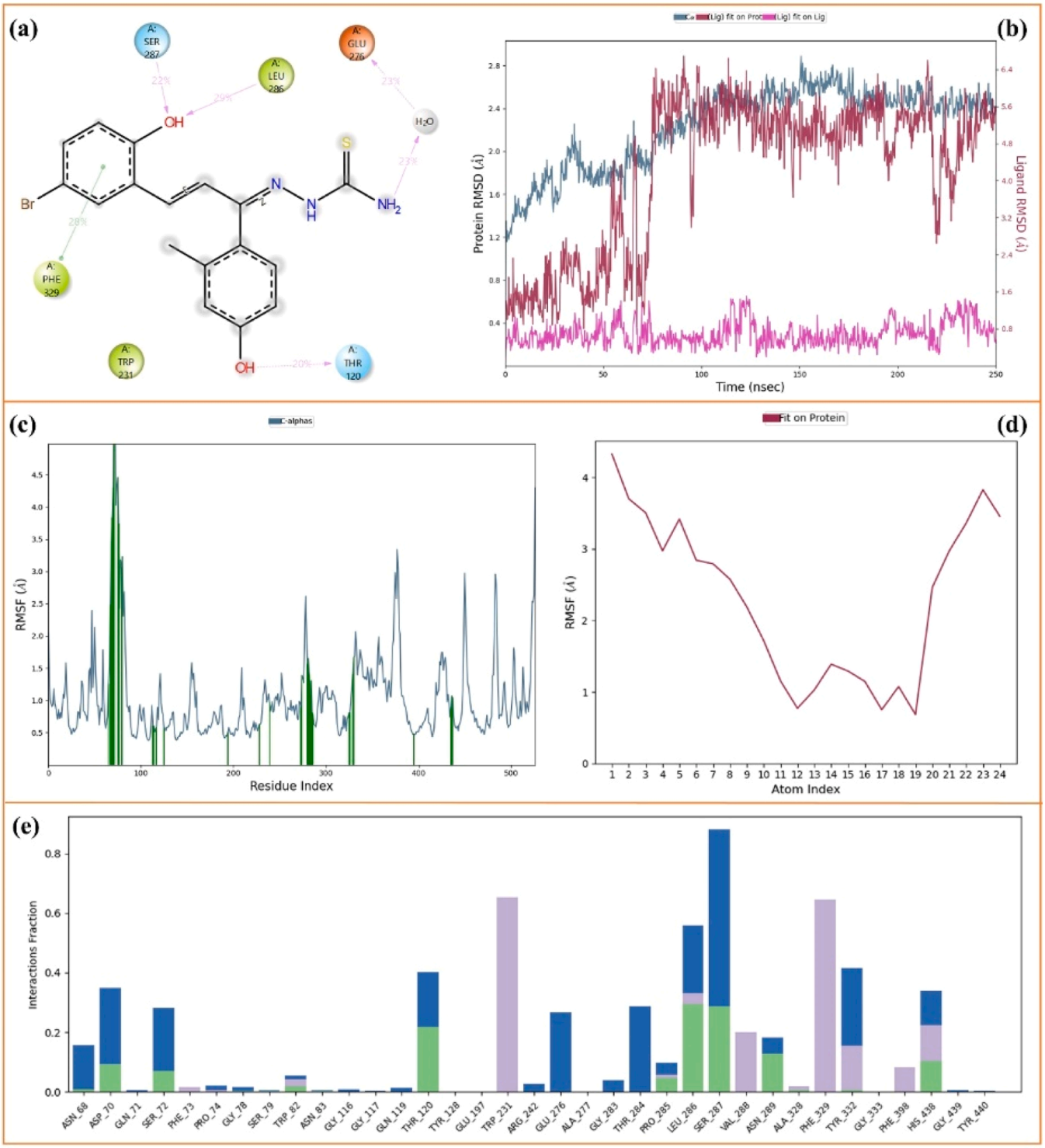


**Fig. 6.** The 250 ns MD simulation analysis of **4-hBChE** complex. (a) 2D key interactions, (b) RMSD values of ligand and protein, (c) RMSF values of protein Cα atoms, (d) RMSF values of ligand atoms, (e) fractional interaction histogram.

atoms were calculated as 1 and 2.5 Å, respectively. While the fluctuations in the protein backbone are quite small, the fluctuations in the ligand atoms are relatively high, causing the RMSD values to increase. Finally, Fig. 7e represents the fractional interaction histogram of 4-hBChE complex during the simulation time. the most abundant fractional interaction histograms were observed with Ser-287, Trp-231, Phe-329 and Leu-286.

### 2.5.3. *MD simulation analysis of 4-αGly complex*

The 250 ns MD simulation analysis of 4-α-Glycosidase complex is given in Fig. 7**,** which represents the 2D key ligand-protein interactions during simulation time. As seen in Fig. 7**a,** the both amino group of thiosemicarbazone moiety formed two hydrogen bond interaction with Gly-228 (96 % and 96 % of the sim.). At the same time the sulfur atom of thiosemicarbazone moiety formed a water-bridged hydrogen bond interaction with Arg-400 (52 % of the sim.) Arg-400 also formed another water-bridged hydrogen bond interaction with imine nitrogen during 63

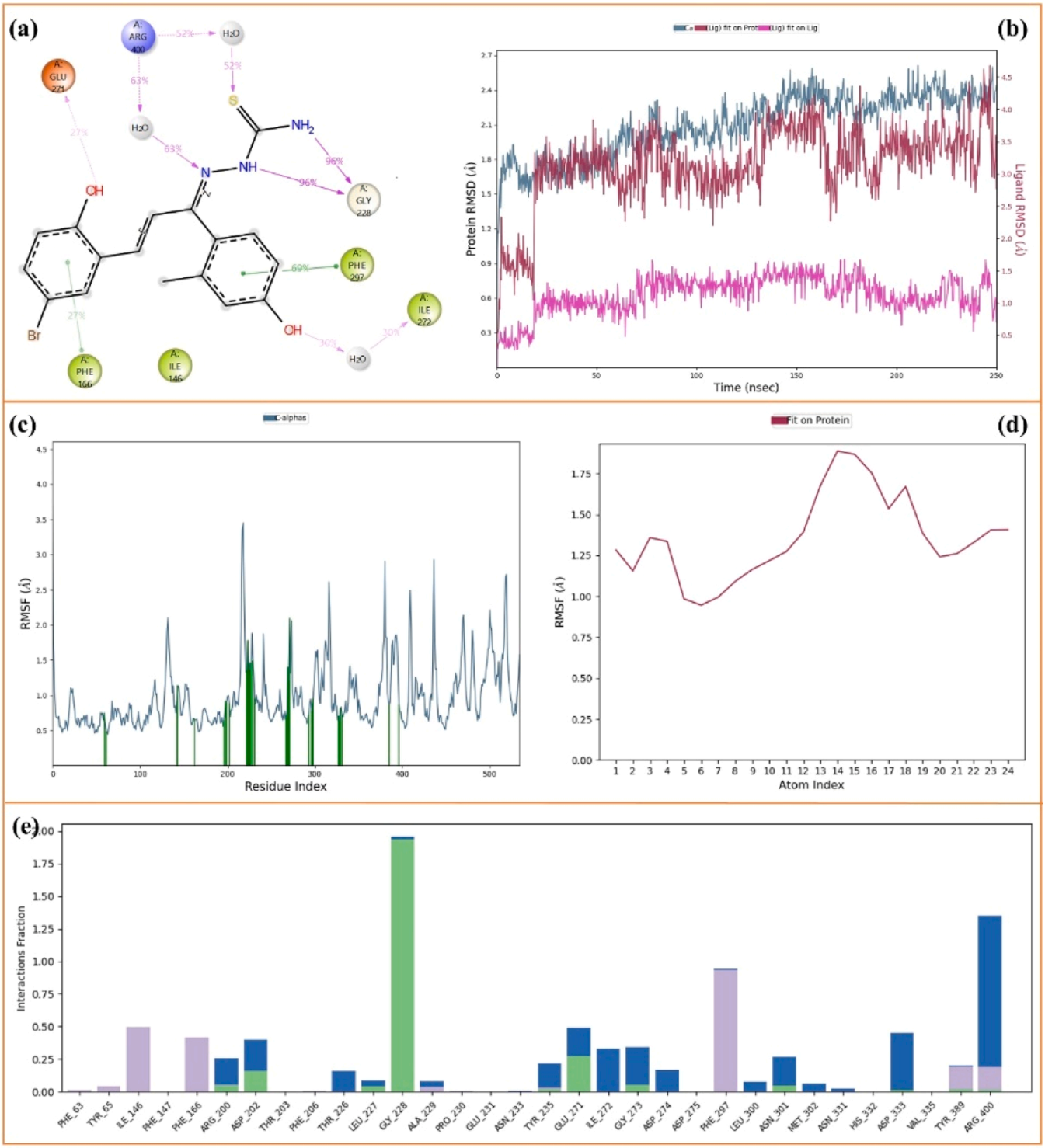


**Fig. 7.** The 250 ns MD simulation analysis of **4-α-Glycosidase** complex. (a) 2D key interactions, (b) RMSD values of ligand and protein, (c) RMSF values of protein Cα atoms, (d) RMSF values of ligand atoms, (e) fractional interaction histogram.

% of the simulation time. While the hydroxyl group of brominated phenyl ring formed a hydrogen bond interaction with Glu-271 (27 % of the sim.) the phenolic hydroxyl group formed a water-bridged hydrogen bond interaction with Ile-272 (30 % of the sim.). Finally, both phenyl ring formed a π-π stacking interaction with Phe-166 (27 % of the sim.) and Phe-297 (69 % of the sim.), separately. The 96 % hydrogen bond interaction between Gly-228 and amino groups greatly increases the stability of this ligand-protein complex. Interactions continue almost throughout the entire simulation time, and other interactions contribute to this stability.

Fig. 7**b** represents the RMSD values of the protein and ligand atoms of **4-α-Glycosidase** complex during simulation time. As seen in Fig. 7**b,** the average RMSD of protein Cα atoms was calculated as 2.2 Å (pale blue). On the other hand, the average RMSD of ligand atoms was calculated as 3 Å (red). The average deviation of ligand from its initial position was calculated as 1 Å. The RMSD values calculated for both protein and ligand atoms are quite reasonable, indicating that the ligand-protein complex is well stable.

Figs. 7**c** and 7**d** represent the RMSF values of protein Cα atoms and ligand atoms, respectively. In Fig. 7**c** the vertical green bars depict the ligand-protein contacts and the average RMSF of the protein Cα atoms was calculated as 1.5 Å. At the same time the average RMSF of ligand atoms was also calculated as 1.5 Å. RMSF values of 1.5 Å for both protein and ligand indicate that the protein backbone and ligand atoms are extremely stable and do not fluctuate throughout the simulation period. Finally, Fig. 7**e** represents the fractional interaction histogram of **4-α-Glycosidase** complex during the simulation time. The most abundant fractional interactions were observed with Gly-228 and Arg-400. Gly-228 is the key amino acid residue for the inhibition of α-Glycosidase for this complex.

### 2.5.4. *MD timeline depiction of protein ligand interaction*

The 250 ns MD simulation timeline depiction of **4-hAChE, 4-hBChE and 4-α-Glycosidase** ligand protein interactions are given in Figs. 8**a,** 8**b** and 8**c** respectively.

The analysis of the MD simulation timelines reveals significant

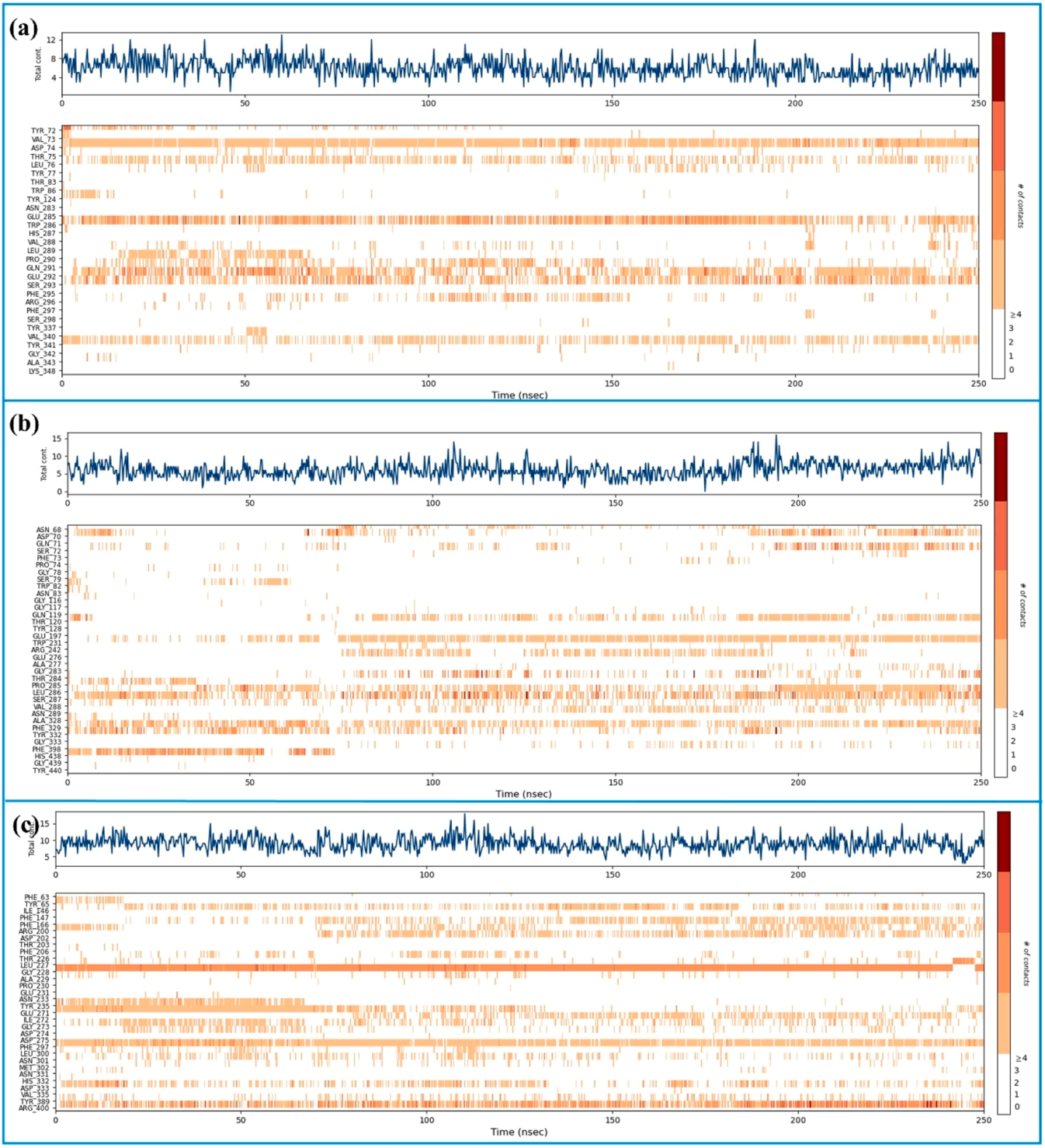


**Fig. 8.** The 250 ns MD simulation analysis of timeline depiction of protein ligand interaction. (a) **4-hAChE** complex, (b) **4-hBChE** complex, (c) **4-α-Glycosidase** complex.

insights into the binding stability and interaction profiles of compound **4** with the three different enzymes. As seen in Fig. 8**a,** compound **4** demonstrates stable binding within the active site of the hAChE enzyme, interacting with amino acid residues Val-73, Glu-285, Gln-291, and Gln-292 throughout the simulation period. Among these, Val-73 and Glu-285 emerge as key amino acid residues. In Fig. 8**b,** the time-dependent interactions of compound **4** with hBChE highlight the longest-lasting interactions with Leu-286 and Ala-328. Compared to the AChE complex, the ligand-protein interactions in the hBChE complex are notably weaker, with shorter binding durations. Finally, in Fig. 8**c,** the most persistent interactions of compound **4** throughout the simulation are observed with amino acid residues Leu-227, Asp-275, and Arg-400. Leu-227 stands out as the primary interacting residue for the entire duration of the simulation. This analysis underscores the importance of MD simulations in elucidating the dynamic interactions between drug compounds and target enzymes, providing critical insights for the rational design of effective therapeutics [47].

As a conclusion of MD simulations of the ligand-protein complexes for **4-hAChE, 4-hBChE,** and **4-αGlycosidase** provided detailed insights into their stability and key interactions. The 250 ns MD simulation of the **4-hAChE** complex revealed critical interactions involving Glu-292, Ser-293, Asp-74, and Tyr-341, with RMSD and RMSF values indicating high stability. Similarly, the **4-hBChE** complex exhibited significant interactions with Ser-287, Leu-286, Thr-120, and Phe-329, maintaining stability throughout the simulation. The **4-αGly** complex showed stable interactions primarily with Gly-228 and Arg-400, demonstrating minimal fluctuations. The consistent RMSD and RMSF values in all simulations highlight the stability of these ligand-protein complexes, highlighting the potentials of compound **4** in drug design and development.

### 2.6. ADME prediction

Absorption, Distribution, Metabolism, and Excretion (ADME) prediction is a critical aspect of drug design, determining the pharmacokinetic profile of potential drug candidates. These properties influence the drug's efficacy, bioavailability, and safety, ensuring that the drug reaches its target in the body at therapeutic concentrations without causing adverse effects. The ADME prediction aimed to assess the compounds' potential as drug candidates and their likelihood of exhibiting favorable pharmacokinetic profiles. Key parameters, such as octanol/water partition coefficient, aqueous solubility, Caco-2 cell permeability, brain/blood partition coefficient, MDCK cell permeability, human oral absorption, and adherence to Lipinski's and Jorgensen's rules, were predicted. The ADME prediction results of all the synthesized compounds are given in Table 3.

According to the Table 3**,** molecular weights of all compounds fall within the acceptable range suggesting they are likely to be orally active. All compounds have QPlogP values within the range of −2.0 to 6.5, indicating balanced lipophilicity for good membrane permeability. The solubility values range from −1.686 to −4.878. Most compounds exhibit high human oral absorption (>80 %), except for compounds **3, 6,** and **7,** which show moderate absorption rates. None of the compounds violate Lipinski and Jorgensen's rules suggesting good drug-likeness and oral bioavailability. Compounds **1, 2, 5,** and **8** show high predicted Caco-2 permeability, MDCK permeability, and %HOA. Compound **4** presence of five hydrogen bond donors and acceptors, balanced lipophilicity with a QPlogP value of +2.917, and acceptable solubility (−4.878). Additionally, it demonstrates high human oral absorption (%84) and does not violate Lipinski's rule of five. Furthermore, its cellular permeability measurements, such as Caco-2 permeability and MDCK permeability, are quite favorable, suggesting good intercellular permeability properties for this compound.

## 3. Conclusions

In this study, a total of nine representatives of acetophenone derivatives **(1–9)** were synthesized. Among them, compounds **2, 4, 5, 6, 7**, and **9** were novel and synthesized for the first time in this study. These compounds span a diverse range of structures, including chalcone derivatives (**1–3**), thiosemicarbazone derivatives (**4–6**), semicarbazone derivative (**7**), and indolone derivatives (**8–9**). The synthesized compounds were subjected to in vitro enzyme inhibition studies against human AChE, human BChE, and α-Glycosidase enzymes. Additionally, their antioxidant capacities were evaluated using the DPPH radical scavenging assay. Notably, compounds **4** and **7** exhibited significant inhibition against all three enzymes, while other compounds demonstrated varying degrees of enzyme inhibition and antioxidant activity.

Molecular docking studies were performed to elucidate the potential binding modes and interactions of the synthesized compounds with the target enzymes (hAChE, hBChE, and α-Glycosidase). The docking scores, MM-GBSA ΔG binding free energies, and Glide Emodel scores provided valuable insights into the binding affinities and inhibitory potentials of the compounds. Compound **4** emerged as a standout candidate, displaying the highest docking scores (for hAChE −12.207, for hBChE −10.140, and for α-Glycosidase −10.590 kcal/mol) against all three enzymes. It's remarkable binding affinities, as evidenced by IFD XP Gscores and MM-GBSA ΔG values, underscore its potential as a potent inhibitor. Furthermore, compound **7**, despite its superior in vitro activity against α-Glycosidase, exhibited notable docking scores, suggesting its potential as a multifunctional inhibitor. The detailed ligand-protein interactions revealed critical hydrogen bonding, π-π stacking, and halogen bonding interactions contributing to the stability of the complexes.

MD simulations were conducted to further investigate the stability and dynamics of the ligand-protein complexes over time. The 250 ns simulations provided valuable insights into the structural integrity and

**Table 3**
ADME prediction of synthesized compounds.

| Comp. | MW | dHB | aHB | QPlogP | QPlogS | QPPCaco | QPlogBB | QPPMDCK | %HOA | Ro5 | Ro3 |
|---|---|---|---|---|---|---|---|---|---|---|---|
| **1** | 224.259 | 1 | 2 | 2.879 | −3.361 | 1130 | −0.643 | 564 | 100 | 0 | 0 |
| **2** | 238.285 | 1 | 2 | 3.180 | −3.976 | 1253 | −0.604 | 631 | 100 | 0 | 0 |
| **3** | 269.256 | 1 | 3 | 2.205 | −3.596 | 134 | −1.669 | 56 | 77 | 0 | 0 |
| **4** | 406.296 | 5 | 5 | 2.917 | −4.878 | 182 | −1.446 | 520 | 84 | 0 | 0 |
| **5** | 207.293 | 3 | 3 | 1.934 | −3.365 | 1134 | −0.377 | 1404 | 92 | 0 | 0 |
| **6** | 191.232 | 3 | 1 | 1.152 | −1.686 | 168 | −1.031 | 163 | 73 | 0 | 0 |
| **7** | 223.292 | 4 | 4 | 1.148 | −2.724 | 369 | −0.883 | 372 | 79 | 0 | 0 |
| **8** | 346.180 | 1 | 4 | 2.942 | −4.195 | 515 | −0.733 | 640 | 92 | 0 | 0 |
| **9** | 297.310 | 1 | 4 | 2.675 | −4.065 | 242 | −1.327 | 106 | 85 | 0 | 0 |

*__MW:__ Molecular weight, 130–722; **dHB:** Number of hydrogen bond donors in an aqueous solution, 0.0 – 6.0; **aHB:** Number of hydrogen bond acceptors in an aqueous solution, 2.0 – 20.0; **QPlogP:** Predicted octanol/water partition coefficient, –2.0 – 6.5; **QPlogS:** Predicted aqueous solubility, –6.5 – 0.5; **QPPCaco:** Predicted apparent Caco-2 cell permeability in nm/*sec*, <25 poor >500 great; **QPlogBB:** Predicted brain/blood partition coefficient, –3.0 – 1.2; **QPPMDCK:** Predicted apparent MDCK cell permeability in nm/*sec*, <25 poor >500 great; **%HOA:** Predicted human oral absorption on 0 to 100 % scale, >80 % is high <25 % is poor; **Ro5:** Number of violations of Lipinski's rule of five, max is 4; **Ro3:** Number of violations of Jorgensen's rule of three, max is 3.

key interactions governing complex stability. Compound **4** consistently demonstrated stable interactions with hAChE, hBChE, and α-Glycosidase throughout the simulation time. The RMSD and RMSF analyses indicated minimal deviations and fluctuations in both the ligand and protein.

The ADME prediction results provided valuable insights into the pharmacokinetic properties and drug-likeness of the synthesized compounds. All compounds exhibited favorable molecular weights, predicted partition coefficients, and permeability characteristics, indicating their potential as orally active agents with good membrane permeability. The adherence to Lipinski's and Jorgensen's rules further supported the drug-likeness of these compounds.

As conclusion, it is possible to suggest that compound **4** has the potential to be a multitarget drug candidate. In vitro enzyme inhibition assays have shown that compound **4** exhibited the highest activity among other compounds, demonstrating strong inhibition against human AChE, human BChE, and α-Glycosidase enzymes. These findings suggest that compound **4** could effectively target these enzymes and potentially be used in the treatment or prevention of neurodegenerative diseases and diabetes.

## 4. Materials and methods

### 4.1. Measurements

$^{1}H$, $^{13}C$ NMR were recorded in acetone-$d_6$ and DMSO-$d_6$ using a Bruker Avance 300 NMR spectrometer (Germany, 300.13 and 75.47 MHz, respectively). The chemical shifts (δ) are given in ppm and referenced to residual solvent: 2.06 ppm (acetone-$d_6$) and 2.50 ppm (DMSO-$d_6$) for $^{1}H$, 29.9 ppm (acetone-$d_6$) and 39.5 ppm (DMSO-$d_6$) respectively. Coupling constants in hertz (Hz) were measured from one-dimensional spectra and multiplicities were abbreviated as following: br (broad), s (singlet), d (doublet), dd (doublet of doublets), m (multiplet). The chemical shifts were recorded in ppm, coupling constants (*J*) in Hz.

### 4.2. Experimental part

All commercially available chemicals were obtained from Merck and Fluka companies and used without further purification. The purity of the synthesized compounds was confirmed by TLC on commercial silica gel plates with an aluminum backing (60 F254), iodine vapor was used as a visualizing agent, eluent hexane-ethyl acetate, 5:3. Melting points were measured on a Stuart SMP30 apparatus without correction. HRMS spectra were recorded using the ESI technique by Thermo Fischer Scientific Q Exactive™ Hybrid Quadrupole-Orbitrap™ Mass Spectrometer. HPLC chromatograms were recorded using the Waters preparative HPLC and PDA detector.

#### 4.2.1. The procedure for the synthesis of chalcones 1–3

The synthesis of chalcones was carried out by Claisen-Schmidt condensation. 0.01 mol of 4-hydroxyacetophenone (or 4-hydroxy-2-methylacetonone) and 0.01 mol of benzaldehyde (or nitrobenzaldehyde) were dissolved in 30 mL of ethanol. The reaction was carried out with a catalytic amount of piperidine for 5 h at room temperature. When the process was completed, the mixture was added to ice and solid part separated from the liquid layer by filtration. After drying, the chalcones were recrystallized from the methanol.

***(2E)−1-(4-hydroxyphenyl)−3-phenylprop-2-en-1-one (1):*** 1.7 g (78 %), yellow crystals, m.p. 91–92 °C; $^{1}H$ NMR (300.13 MHz, DMSO-$d_6$) δ: 8.57 (br s, 1H, OH), 7.74–6.68(m, 11H, Ph-H and CH═CH).

***(2E)−1-(4-hydroxy-2-methylphenyl)−3-phenylprop-2-en-1-one (2):*** 1.6 g (67 %), yellow crystals, m.p. 95–97 °C; $^{1}H$ NMR (300.13 MHz, acetone-$d_6$) δ: 9.04 (br s, 1H, OH), 7.73–7.43 (m, 9H, Ph-H and CH=), 6.79 (d, $J = 14.9$ Hz, 1H, CH=), 2.47 (s, 3H, $CH_3$); $^{13}C$ NMR (75.47 MHz, acetone-$d_6$) δ: 192.0 (CO), 159.8 (C), 143.0, 141.1 (C), 135.3 (C), 131.8, 130.1, 128.9, 128.3, 125.9, 120.0, 118.4 (C), 112.2, 20.5. ESI-HRMS: *m/z* Formula: $C_{16}H_{14}O_2$, Calculated $[M\text{-}H]^+$: 237.09155, Found $[M\text{-}H]^+$: 237.09190; HPLC-PDA: λ 254 nm, MeCN:MeOH (1:1), Rt: 3.29 min, 97.55 %.

***(2E)−1-(4-hydroxy-2-methylphenyl)−3-(4-nitrophenyl)prop-2-en-1-one (3):*** 2.5 g (87 %), yellow crystals, m.p. 122–124 °C; $^{1}H$ NMR (300.13 MHz, DMSO-$d_6$) δ: 9.90 (br s, 1H, OH), 8.24 (d, $J = 7.9$ Hz, 2H, Ph-H), 7.97 (d, $J = 7.9$ Hz, 2H, Ph-H), 7.73–7.51 (m, 4H, Ph-H and CH=), 6.70 (d, $J = 14.9$ Hz, 1H, CH=), 244 (s, 3H, $CH_3$); $^{13}C$ NMR (75.47 MHz, DMSO-$d_6$) δ: 190.6 (CO), 161.1 (C), 148.2 (C), 139.7 (C), 132.6, 129.8, 129.5, 128.9 (C), 124.1 (C), 122.8, 118.9, 112.6, 21.8.

#### 4.2.2. The procedure for the synthesis of thiosemicarbazones (4–6) and semicarbazone (7)

A mixture of 0.01 mmol thiosemicarbazide and 0.01 mol (2*E*)−3-(5-bromo-2-hydroxyphenyl)−1-(4-hydroxyphenyl)prop-2-en-1-one (in other cases, (2*E*)−1-(4-methylphenyl)−3-phenylprop-2-en-1-one or (2*E*)−1-(4-hydroxy-2-methylphenyl)−3-phenylprop-2-en-1-one) was stirred in 30 mL DMSO (at 110–115 °C) for 3 h. After cooling to 20–25 °C, the reaction mixture was added to ice and solid part separated from the liquid layer by filtration. The precipitate was filtered off, washed with water and dried. The obtained thiosemicarbazones **4, 5** and **6** were purified by recrystallization from the DMSO-ethanol mixture 1:5. The synthesis of semicarbazone **7** was performed by a similar method in the presence of semicarbazide.

***(2E)−2-[(2E)−3-(5-bromo-2-hydroxyphenyl)−1-(4-hydroxy-2-methylphenyl)prop-2-en-1-ylidene]hydrazinecarbothioamide (4):*** 2.3 g (57 %), light yellow crystals, m.p. 133–135 °C; $^{1}H$ NMR (300.13 MHz, DMSO-$d_6$) δ: 10.15 (s, 1H, NH), 9.83 (s, 1H, OH), 8.54 (s, 1H, OH), 8.18 (s, 1H, Ph-H), 8.10 (s, 2H, $NH_2$), 7.55 (s, 1H, Ph-H), 7.22–6.77 (m, 5H, Ph-H and CH═CH), 6.51 (d, $J = 14.7$ Hz, 1H, CH=), 2.00 (s, 3H, $CH_3$); $^{13}C$ NMR (75.47 MHz, DMSO-$d_6$) δ: 177.9 (CS), 158.9 (C), 154.9 (C), 157.2 (C), 137.6 (C), 133.6 (C), 132.4, 130.8 (C), 130.1, 129.6, 125.5, 120.4, 118.5, 118.0, 111.5, 111.1 (C), 19.32. ESI-HRMS: *m/z* Formula: $C_{17}H_{16}BrN_3O_2S$, Calculated $[M\text{-}H]^+$: 404.00684, Found $[M\text{-}H]^+$: 404.00745; HPLC-PDA: λ 254 nm, MeCN:MeOH (1:1), Rt: 3.75 min, 95.49 %.

***(2E)−2-[1-(4-methylphenyl)ethylidene]hydrazinecarbothioamide (5):*** 1.7 g (81 %), white yellow crystals, m.p. 143–144 °C; $^{1}H$ NMR (300.13 MHz, DMSO-$d_6$) δ: 9.32 (s, 1H, NH), 7.71 (d, $J = 7.7$ Hz, 2H, Ph-H), 7.18 (d, $J = 7.7$ Hz, 2H, Ph-H), 6.49 (br s, 2H, $NH_2$), 2.31 (s, 3H, $CH_3$), 2.16 (s, 3H, $CH_3$); $^{13}C$ NMR (75.47 MHz, DMSO-$d_6$) δ: 157.9 (C), 144.5 (C), 138.3 (C), 135.9 (C), 129.2, 126.3, 21.2, 13.7. ESI-HRMS: *m/z* Formula: $C_{10}H_{13}N_3S$, Calculated $[M\text{-}H]^+$: 206.07519, Found $[M\text{-}H]^+$: 206.07553; HPLC-PDA: λ 254 nm, MeCN:MeOH (1:1), Rt: 3.03 min, 99.18 %.

***(2E)−2-[1-(2-hydroxy-4-methylphenyl)ethylidene]hydrazinecarbothioamide (6):*** 1.3 g (58 %), yellow crystals, m.p. 145–147 °C; $^{1}H$ NMR (300.13 MHz, DMSO-$d_6$) δ: 9.74 (s, 1H, NH), 8.30 (s, 1H, OH), 8.05 and 7.82 (s, 2H, $NH_2$), 6.98 (d, $J = 7.8$ Hz, 2H, Ph-H), 6.75–6.72 (m, 3H, Ph-H), 2.14 (s, 3H, $CH_3$), 2.04 (s, 3H, $CH_3$); $^{13}C$ NMR (75.47 MHz, DMSO-$d_6$) δ: 179.2 (CS), 157.8 (C), 151.7 (C), 137.4 (C), 130.2, 117.8, 114.3 (C), 21.1, 18.7.

***(2E)−2-[1-(4-methylphenyl)ethylidene]hydrazinecarboxamide (7):*** 1.2 g (63 %), white crystals, m.p. 138–139 °C; $^{1}H$ NMR (300.13 MHz, acetone-$d_6$) δ: 9.85 (s, 1H, NH), 7.95 (s, 2H, $NH_2$), 7.85 (d, $J = 7.7$ Hz, 2H, Ph-H), 7.2 (d, $J = 7.7$ Hz, 2H, Ph-H), 2.35 (s, 3H, $CH_3$), 2.18 (s, 3H, $CH_3$); $^{13}C$ NMR (75.47 MHz, acetone-$d_6$) δ: 179.9 (CS), 147.3 (C), 139.7 (C), 137.7 (C), 129.1, 127.2, 19.9, 14.8. ESI-HRMS: *m/z* Formula: $C_{10}H_{12}N_3O$, Calculated $[M\text{-}H]^+$: 190.09804, Found $[M\text{-}H]^+$: 190.09844; HPLC-PDA: λ 254 nm, MeCN:MeOH (1:1), Rt: 3.07 min, 99.56 %.

#### 4.2.3. The procedure for the synthesis of indolones 8 and 9

A mixture of 0.01 mol isatin, 0.01 mol) 4-bromoacetophenone (or 4-hydroxy-2-methylacetophenone) and 0.5 mL diethylamine in 30 mL ethanol was stirred at 75–78 °C for 1 h. After cooling to 20–25 °C, the

reaction mixture was added to ice and solid part separated from the liquid layer by filtration. The precipitate was filtered off, washed with water and dried. The obtained indolones 8 and 9 were purified by recrystallization from the methanol.

***3-(4-Bromobenzyl)−3-hydroxy-1,3-dihydro-2H-indol-2-one (8):*** 2.3 g (66 %), brown powder, m.p. 140–141 °C; $^{1}$H NMR (300.13 MHz, DMSO-$d_6$) δ: 10.21 (s, 1H, NH), 7.80 (d, $J$ = 7.4 Hz, 2H, Ph-H), 7.71 (d, $J$ = 7.4 Hz, 2H, Ph-H), 7.25–6.87 (m, 4H, Ph-H), 6.09 (s, 1H, OH), 4.04 and 3.55 (d, $J$ = 18 Hz, 2H, $CH_2$); $^{13}$C NMR (75.47 MHz, DMSO-$d_6$) δ: 196.2 (CO), 178.7 (CO), 143.3 (C), 135.6 (C), 135.3 (C), 132.2 (C), 130.5, 129.5, 128.1, 124.1, 121.6, 109.9, 73.4, 46.2.

***3-Hydroxy-3-(2-hydroxy-5-methylbenzyl)−1,3-dihydro-2H-indol-2-one (9):*** 2.2 g (73 %), brown powder, m.p. 158–159 °C; $^{1}$H NMR (300.13 MHz, acetone-$d_6$) δ: 11.51 (s, 1H, OH), 10.17 (s, 1H, NH), 7.81 (s, 1H, Ph-H), 7.33–6.79 (m, 5H, Ph-H), 5.97 (s, 1H, OH), 4.12 and 3.69 (d, $J$ = 18 Hz, 2H, $CH_2$), 2.31 (s, 3H, $CH_3$); $^{13}$C NMR (75.47 MHz, acetone-$d_6$) δ: 203.2 (CO), 178.5 (CO), 159.6 (C), 143.4 (C), 137.5, 131.9 (C), 130.8, 129.1(C), 128.2, 123.4, 121.3, 119.7 (C), 117.7, 109.9, 73.4, 46.3, 19.7. ESI-HRMS: *m/z* Formula: $C_{17}H_{15}NO_4$, Calculated $[M-H]^+$: 296.09228, Found $[M-H]^+$: 296.09256; HPLC-PDA: λ 190 nm, MeCN:MeOH (1:1), Rt: 2.85 min, 95.86 %.

### 4.3. Computational studies

Molecular Docking studies using carried out by Schrödinger Molecular Modelling Software (2024–1) with Maestro (13.9) interface. MD simulations were carried out using Desmond (D. E. Shaw Research) with Maestro (13.5) interface.

#### 4.3.1. Preparation of ligands and proteins

The known methods that previously published by our research group were used to perform protein and ligand preparation [2]. The 3D X-ray crystallographic structures of the target proteins were obtained from the Protein Data Bank, accessible via the RCSB website (https://www.rcsb.org). In this study, hAChE (PDB ID: 4M0E), hBChE (PDB ID: 5NN0), and α-Glycosidase (PDB ID: 3WY1) were used to carried out for all *in silico* studies. Careful preparation and refinement of these protein structure was carried out using the Protein Preparation Wizard module within Schrödinger Maestro 13.9 [48].

#### 4.3.2. Glide docking and induced fit docking

The known methods that previously published by our research group were used to perform glide docking and induced fit docking. The ligands we prepared were subjected to docking into the respective receptors using the IFD protocol, part of the Schrödinger suite (Schrödinger Release 2024–1, Induced Fit Docking protocol, Glide, Schrödinger, LLC, New York, NY). The center of the Glide grid was determined based on the native ligand's centroid, with the inner box side set at 25 Å, and the outer box side was automatically defined. 20 poses for each ligand were derived according to the standard IFD protocol, and each pose was docked with Glide XP docking sensitivity. Finally, IFD docking scores, representing the binding energy, was computed for each generated pose [49].

#### 4.3.3. Prime MM-GBSA analysis

The known methods that previously published by our research group were used to perform prime MM-GBSA analysis. The free binding energy between the ligand and protein in the docked poses was calculated using the Prime MM-GBSA module within the Schrödinger suite 2024–1, following methods described in previous publications [42,50]. Default parameters, such as the VSGB solvation model and Minimize sampling method, were used in the MM/GBSA module. During the energy calculation, specific residues surrounding the receptor pocket were constrained to maintain flexible conformations.

#### 4.3.4. Molecular dynamics simulations

The known methods that previously published by our research group were used to perform molecular dynamics simulations. The protein-ligand complex was built using the Desmond system builder, then placed in a simulation box with a 10 Å buffer zone. Water (Tip3p model) and NaCl (0.15 M) were added to neutralize the system. The OPLS3 force field was used for energy minimization. A 100 ns molecular dynamics simulation at 300 °K and 1 bar pressure was run with a 100 ps time step using Desmond. Interactions between the ligand and protein were analyzed, and RMSD values for protein Cα atoms and ligand heavy atoms were calculated to assess stability during simulation time [51].

#### 4.3.5. ADME prediction

The in silico ADME properties of the selected compounds were performed utilized the QikProp panel of Maestro 13.5. QikProp provides values that compare the properties of new molecules to 95 % of known drugs [52,53].

### 4.4. Biological assays

#### 4.4.1. AChE and BCHE methods

The Ellman's method [49] was used to investigate how newly discovered chemicals influenced AChE/BChE activity. To measure the AChE/BChE activity, DTNB (Product No D8130–1 G, Sigma-Aldrich) and AChI/BChI were utilized as substrates. To be exact, 100 μL of buffer (Tris/HCl, 1 M, pH 8.0) was used to dissolve multiple volumes of the sample solution (10 mL). Following the addition of the AChE/BChE ($5.32 \times 10^3$ EU) solution, 50 μL was incubated at 25 °C for 10 min [50]. Following the incubation period, 50 μL of 0.5 mM DTNB was added. Finally, 50 mL of AChI/BChI (10 mM, Product no: 01,480–1 G, Sigma-Aldrich) was added to start the reaction. By observing the spectrophotometric creation of the yellow 5-thio-2-nitrobenzoate anion at a wavelength of 412 nm, which is produced when DTNB combines with thiocholine, the enzymatic hydrolysis of both substrates was quantified [51]. Different concentrations of the novel compounds were added to the reaction mixture to see how they affected AChE. Next, the AChE/BChE activity were assessed. Activity (%) vs. compound plots were used to obtain the $IC_{50}$ values.

#### 4.4.2. α-Glycosidase assay

Following the methodology of Tao et al. [52] the activity of the compounds on α-Glycosidase was evaluated using the substrate p-NPG. 20 mg were dissolved in 20 mL of EtOH:$H_2O$ to make samples. First, 700 μL of pH 7.4 phosphate buffer (0.15 u/mL), 20 μL of enzyme solution, and 5–200 μL of sample were mixed together. After pre-incubating for 10 min at 35 °C, 50 μL of p-NPG was added to the reaction. Furthermore, following the pre-incubation, 50 μL of p-NPG in phosphate buffer (5 mM, pH 7.4) was added, and the experiment was repeated at 35 °C. From the data, curve fitting was utilized to calculate the $IC_{50}$ and $K_i$ values. We used the chemical acarbose as a positive control. Spectrophotometry was used to determine the absorbances at 405 nm [53].

#### 4.4.3. DPPH radical scavenging assay

According to Blois's spectroscopic approach, the compounds' DPPH radical scavenging activity was ascertained [54]. A new 0.1 M DPPH radical solution was made in ethanol, to put it briefly. Next, a 0.5 mL aliquot of this solution (10–30 μg/mL) was mixed with 1.5 mL of olivetol in ethanol. After thoroughly combining these mixes, they were left to incubate for 30 min in the dark. And lastly, using a spectrophotometer, the absorbance value was measured at 517 nm [56].

## CRediT authorship contribution statement

**Aynur Farzaliyeva:** Methodology, Investigation. **Halil Şenol:** Writing – original draft, Methodology, Investigation. **Parham Taslimi:** Writing – review & editing, Methodology, Investigation, Formal

analysis. **Furkan Çakır:** Formal analysis, Methodology. **Vagif Farzaliyev:** Writing – original draft, Software, Methodology. **Nastaran Sadeghian:** Writing – original draft, Methodology, Investigation. **Ibrahim Mamedov:** Software, Methodology, Investigation. **Afsun Sujayev:** Writing – review & editing, Methodology. **Abel Maharramov:** Writing – original draft, Methodology, Investigation. **Saleh Alwasel:** Writing – original draft, Project administration, Funding acquisition. **İlhami Gulçin:** Writing – review & editing, Investigation.

## Declaration of competing interest

The authors declare that they have no known competing financial interests or personal relationships that could have appeared to influence the work reported in this paper.

## Data availability

Data will be made available on request.

## Acknowledges

Saleh Alwasel wishes to express his heartfelt gratitude to King Saud University's Researchers Supporting Project (RSP-2024/59).

This paper was supported by Baku State University, Bezmialem Vakif University, Bartin University, Azerbaijan Institute of Chemistry of Additives, King Saud University and Atatürk University.

## Supplementary materials

Supplementary material associated with this article can be found, in the online version, at doi:10.1016/j.molstruc.2024.140197.

## References

[1] F.S. Tokalı, P. Taslimi, B. Tuzun, A. Karakuş, N. Sadeghian, İ. Gulçin, Novel quinazolinone derivatives: potential synthetic analogs for the treatment of glaucoma, alzheimer's disease and diabetes mellitus, Chem. Biodivers. 20 (10) (2023) e202301134, https://doi.org/10.1002/cbdv.202301134.

[2] H. Şenol, M. Ghaffari-Moghaddam, G.Ö. Alim Toraman, U. Güller, Novel chalcone derivatives of ursolic acid as acetylcholinesterase inhibitors: synthesis, characterization, biological activity, ADME prediction, molecular docking and molecular dynamics studies, J. Mol. Struct. 1295 (2024) 136804, https://doi.org/10.1016/j.molstruc.2023.136804.

[3] P. Taslimi, H. Akincioglu, I. Gulcin, Synephrine and phenylephrine act as α-amylase, α-glycosidase, acetylcholinesterase, butyrylcholinesterase, and carbonic anhydrase enzymes inhibitors, J. Biochem. Mol. Toxic. 31 (11) (2017) e21973, https://doi.org/10.1002/jbt.21973.

[4] H. Şenol, Ö. Özgun-Acar, A. Dağ, A. Eken, H. Güner, Z.G. Aykut, G. Topçu, A. Şen, Synthesis and comprehensive in vivo activity profiling of olean-12-en-28-ol, 3β-pentacosanoate in experimental autoimmune encephalomyelitis: a natural remyelinating and anti-inflammatory agent, J. Nat. Prod. 86 (1) (2023) 103–118, https://doi.org/10.1021/acs.jnatprod.2c00798.

[5] F.S. Tokalı, P. Taslimi, B. Tüzün, A. Karakuş, N. Sadeghian, İ. Gulçin, Synthesis of new carboxylates and sulfonates containing thiazolidin-4-one ring and evaluation of inhibitory properties against some metabolic enzymes, J. Iran. Chem. Soc. 20 (10) (2023) 2631–2642, https://doi.org/10.1007/s13738-023-02861-3.

[6] H. Şenol, 4-Furfuryloxymethyl-1,2,3-triazol-1-yl-acetohydrazide hybrids as cholinesterase and carbonic anhydrase inhibitors: synthesis, characterization and comprehensive biological activity studies, ChemistrySelect 9 (6) (2024) e202303927, https://doi.org/10.1002/slct.202303927.

[7] P. Scheltens, B. De Strooper, M. Kivipelto, H. Holstege, G. Chetelat, C.E. Teunissen, J. Cummings, W.M. van der Flier, Alzheimer's disease, Lancet 397 (10284) (2021) 1577–1590, https://doi.org/10.1016/s0140-6736(20)32205-4.

[8] H. Şenol, G. Çelik Turgut, A. Şen, R. Sağlamtaş, S. Tuncay, İ. Gülçin, G. Topçu, Synthesis of nitrogen-containing oleanolic acid derivatives as carbonic anhydrase and acetylcholinesterase inhibitors, Med. Chem. Res. 32 (4) (2023) 694–704, https://doi.org/10.1007/s00044-023-03031-z.

[9] F.S. Tokalı, P. Taslimi, İ.H. Demircioğlu, K. Şendil, B. Tuzun, İ. Gülçin, Novel phenolic Mannich base derivatives: synthesis, bioactivity, molecular docking, and ADME-Tox Studies, J. Iran. Chem. Soc. 19 (2) (2022) 563–577, https://doi.org/10.1007/s13738-021-02331-8.

[10] I. Gulcin, B. Trofimov, R. Kaya, P. Taslimi, L. Sobenina, E. Schmidt, O. Petrova, S. Malysheva, N. Gusarova, V. Farzaliyev, A. Sujayev, S. Alwasel, C.T. Supuran, Synthesis of nitrogen, phosphorus, selenium and sulfur-containing heterocyclic compounds - Determination of their carbonic anhydrase, acetylcholinesterase, butyrylcholinesterase and alpha-glycosidase inhibition properties, Bioorg. Chem. 103 (2020) 104171, https://doi.org/10.1016/j.bioorg.2020.104171.

[11] İ. Gulcin, O.V. Petrova, P. Taslimi, S.F. Malysheva, E.Y. Schmidt, L.N. Sobenina, N. K. Gusarova, B.A. Trofimov, B. Tuzun, V.M. Farzaliyev, S. Alwasel, A.R. Sujayev, Synthesis, characterization, molecular docking, acetylcholinesterase and α-glycosidase inhibition profiles of nitrogen-based novel heterocyclic compounds, ChemistrySelect 7 (19) (2022) e202200370, https://doi.org/10.1002/slct.202200370.

[12] I. Gulcin, S.H. Alwasel, Metal ions, metal chelators and metal chelating assay as antioxidant method, Processes 10 (1) (2022) 132, https://doi.org/10.3390/pr10010132.

[13] U. Kolak, I. Hacibekiroglu, M. Ozturk, F. Ozgokce, G. Topcu, A. Ulubelen, Antioxidant and anticholinesterase constituents of *Salvia poculata*, Turk. J. Chem. 33 (6) (2009) 813–823, https://doi.org/10.3906/kim-0902-15.

[14] A. Ulubelen, U. Sonmez, G. Topcu, Diterpenoids from the roots of *Salvia sclarea*, Phytochemistry 44 (7) (1997) 1297–1299, https://doi.org/10.1016/s0031-9422(96)00709-1.

[15] H. Nazemiyeh, F. Bahadori, A. Delazar, M. Ay, G. Topcu, L. Nahar, R.R.T. Majinda, S.D. Sarker, Antioxidant phenolic compounds from the leaves of *Erica arborea* (Ericaceae), Nat. Prod. Res. 22 (16) (2008) 1385–1392, https://doi.org/10.1080/14786410701824007.

[16] O.g.V. Petrova, D.N. Tomilin, H. Şenol, K.V. Belyaeva, L.P. Nikitina, L.A. Oparina, L.N. Sobenina, B.A. Trofimov, N. Sadeghian, P. Taslimi, V. Farzaliyev, A. Sujayev, İ. Gulçin, Synthesis of pyrrole-heterocyclic derivatives as anti-Alzheimer and antidiabetic candidates: an in vitro-in silico study, J. Mol. Struct. 1315 (2024) 138998, https://doi.org/10.1016/j.molstruc.2024.138998.

[17] G.Ö.Alim Toraman, S. Atasoy, H. Şenol, E.Ş. Okudan, H.Ö. Dinç, G. Topçu, LC-MS and GC–MS analyses on green algae *Penicillus capitatus*: cytotoxic, antimicrobial and anticholinesterase activity screening enhanced by molecular docking & dynamics and ADME studies, Chem. Biodivers. (2024) e202400915, https://doi.org/10.1002/cbdv.202400915.

[18] V.-H. Le, V.T. Kim Lien, V.T. Pham, Q.T. Tran, P.T. Thuy, C.V. Ha, V.V. Doanh, L. T. Ha, C.H. Hanh, P.N. Thao, N.-Q. Luc, Effect of extended π-conjugation on photophysical characteristics of chalcone and cinnamylideneacetophenone, Mater. Sci. Semicond. Process. 162 (2023) 107507, https://doi.org/10.1016/j.mssp.2023.107507.

[19] E.P. Mendes, C.M. Goulart, O.A. Chaves, V.d.S. Faiões, M.M. Canto-Carvalho, G. C. Machado, E.C. Torres-Santos, A. Echevarria, Evaluation of novel chalcone-thiosemicarbazones derivatives as potential anti-leishmania amazonensis agents and its HSA binding studies, Biomolecules (2019).

[20] N. Georgiou, A. Katsogiannou, D. Skourtis, H. Iatrou, D. Tzeli, S. Vassiliou, U. Javornik, J. Plavec, T. Mavromoustakos, Conformational properties of new thiosemicarbazone and thiocarbohydrazone derivatives and their possible targets, Molecules 27 (8) (2022) 2537, https://doi.org/10.3390/molecules27082537.

[21] J.G. Da Silva, C.C.H. PerdigÃO, N.L. Speziali, H. Beraldo, Chalcone-derived thiosemicarbazones and their zinc(II) and gallium(III) complexes: spectral studies and antimicrobial activity, J. Coord. Chem. 66 (3) (2013) 385–401, https://doi.org/10.1080/00958972.2012.757762.

[22] D. Hu, N. Zhang, Y. Zhang, C. Yuan, C. Gong, Y. Zhou, W. Xue, Design, synthesis and biological activity of novel chalcone derivatives containing indole, Arab. J. Chem. 16 (6) (2023) 104776, https://doi.org/10.1016/j.arabjc.2023.104776.

[23] J. Yan, Y. Xu, X. Jin, Q. Zhang, F. Ouyang, L. Han, M. Zhan, X. Li, B. Liang, X. Huang, Structure modification and biological evaluation of indole-chalcone derivatives as anti-tumor agents through dual targeting tubulin and TrxR, Eur. J. Med. Chem. 227 (2022) 113897, https://doi.org/10.1016/j.ejmech.2021.113897.

[24] N. Maciejewska, M. Olszewski, J. Jurasz, M. Serocki, M. Dzierzynska, K. Cekala, E. Wieczerzak, M. Baginski, Novel chalcone-derived pyrazoles as potential therapeutic agents for the treatment of non-small cell lung cancer, Sci. Rep. 12 (1) (2022) 3703, https://doi.org/10.1038/s41598-022-07691-6.

[25] T. Constantinescu, A.G. Mihis, Two important anticancer mechanisms of natural and synthetic chalcones, Int. J. Mol. Sci. 23 (19) (2022) 11595, https://doi.org/10.3390/ijms231911595.

[26] N.A.A. Elkanzi, H. Hrichi, R.A. Alolayan, W. Derafa, F.M. Zahou, R.B. Bakr, Synthesis of chalcones derivatives and their biological activities: a Review, ACS Omega 7 (32) (2022) 27769–27786, https://doi.org/10.1021/acsomega.2c01779.

[27] E. Madbouly, E.-S. Lashine, A. Al-Karmalawy, M. Sebaiy, H. Pratsinis, D. Kletsas, K. Metwally, Design and synthesis of novel quinazolinone-chalcone hybrids as potential apoptotic candidates targeting caspase-3 and PARP-1: in vitro, molecular docking, and SAR studies, New J. Chem. 46 (2022) 22013–22029, https://doi.org/10.1039/D2NJ04053K.

[28] H. Şenol, M. Ghaffari-Moghaddam, Ş. Bulut, F. Akbaş, A. Köse, G. Topçu, Synthesis and anticancer activity of novel derivatives of α,β-unsaturated ketones based on oleanolic acid: in vitro and in silico studies against prostate cancer cells, Chem. Biodivers. 20 (9) (2023) e202301089, https://doi.org/10.1002/cbdv.202301089.

[29] G. Thirunarayanan, K.G. Sekar, Solvent-free one-pot cyclization and acetylation of chalcones: synthesis of some 1-acetyl pyrazoles and spectral correlations of 1-(3-(3,4-dimethylphenyl)-5-(substituted phenyl)-4,5-dihydro-1H-pyrazole-1-yl) ethanones, J. Saudi Chem. Soc. 20 (6) (2016) 661–672, https://doi.org/10.1016/j.jscs.2013.12.002.

[30] F.S. Tokalı, H. Şenol, T.G. Katmerlikaya, A. Dağ, K. Şendil, Novel thiosemicarbazone and thiazolidin-4-one derivatives containing vanillin core: synthesis, characterization, and anticancer activity studies, J. Heterocycl. Chem. 60 (4) (2023) 645–656, https://doi.org/10.1002/jhet.4619.

[31] R. Patil, S.A. Patil, K.D. Beaman, S.A. Patil, Indole molecules as inhibitors of tubulin polymerization: potential new anticancer agents, an update (2013-2015),

Future Med. Chem. 8 (11) (2016) 1291–1316, https://doi.org/10.4155/fmc-2016-0047.
[32] M.N. Semenova, D.V. Demchuk, D.V. Tsyganov, N.B. Chernysheva, A.V. Samet, E. A. Silyanova, V.P. Kislyi, A.S. Maksimenko, A.E. Varakutin, L.D. Konyushkin, M. M. Raihstat, A.S. Kiselyov, V.V. Semenov, Sea urchin embryo model as a reliable in vivo phenotypic screen to characterize selective antimitotic molecules. comparative evaluation of combretapyrazoles, -isoxazoles, -1,2,3-triazoles, and -pyrroles as tubulin-binding agents, ACS Comb. Sci. 20 (12) (2018) 700–721, https://doi.org/10.1021/acscombsci.8b00113.
[33] K.S. Kumar, S. Mohanty, G.P. Reddy, V. Siddaiah, J.D. Lilakar, G.L. Goud, Synthesis and antimicrobial activity of 3-{2- (1-Aryl-1H-1,2,3-triazol-4-yl)methoxy -5-fluorophenyl}isoxazoles, Russ. J. Gen. Chem. 89 (6) (2019) 1221–1224, https://doi.org/10.1134/s1070363219060197.
[34] A. Thiriveedhi, R. Venkata Nadh, N. Srinivasu, K. Kaushal, Novel hybrid molecules of isoxazole chalcone derivatives: synthesis and study of in vitro cytotoxic activities, Lett. Drug. Des. Discov. 15 (6) (2018) 576–582, https://doi.org/10.2174/1570180814666170914121740.
[35] J.R. Dimmock, K.K. Sidhu, S.D. Tumber, S.K. Basran, M. Chen, J.W. Quail, J. Yang, I. Rozas, D.F. Weaver, Some aryl semicarbazones possessing anticonvulsant activitie, Eur. J. Med. Chem. 30 (4) (1995) 287–301, https://doi.org/10.1016/0223-5234(96)88237-7.
[36] S. Li, Z. Xie, X. Bian, C. Wang, New Synthesis of 1,3-diaryl-4-nitro-1-butanones by microwave-promoted michael addition of nitromethane to chalcones without solvent, J. Chem. Res. 2007 (11) (2007) 660–661, https://doi.org/10.3184/030823407X266199.
[37] A.C. Kavale, A.H. Kalbandhe, I.A. Opai, A.A. Jichkar, N.N. Karade, Oxidative ring expansion of 3-hydroxy-3-phenacyloxindoles using phenyliodine diacetate and molecular iodine: synthesis of 2-hydroxy-2-aryl/alkyl-2,3-dihydroquinolin-4(1H)-ones, Tetrahedron Lett. 62 (2021) 152631, https://doi.org/10.1016/j.tetlet.2020.152631.
[38] G.G. Abbasova, R.H. Ismayilov, D.B. Tagiyev, H. Şenol, Y. Song, A.A. Medjidov, M. T. Huseynova, P.A. Fatullaeva, P. Taslimi, N. Sadeghian, G.-H. Lee, S.-M. Peng, Synthesis, characterization, crystal structure, molecular dynamics simulations, MM-GBSA analysis, and bioactivity studies of pyrazine- and pyrimidine-modulated unsymmetrical dipyridylamide complexes, J. Mol. Struct. 1315 (2024) 138896, https://doi.org/10.1016/j.molstruc.2024.138896.
[39] E. Farzaneh, M. Mohammadi, P. Raymand, M. Noori, S. Golestani, S. Ranjbar, Y. Ghasemi, M. Mohammadi-Khanaposhtani, M. Asadi, E. Nasli Esfahani, H. Rastegar, B. Larijani, M. Mahdavi, P. Taslimi, Pyrano[2,3-b]chromone derivatives as novel dual inhibitors of α-glucosidase and α-amylase: design, synthesis, biological evaluation, and in silico studies, Bioorg. Chem. 145 (2024) 107207, https://doi.org/10.1016/j.bioorg.2024.107207.
[40] T.I. Adelusi, A.-Q.K. Oyedele, I.D. Boyenle, A.T. Ogunlana, R.O. Adeyemi, C. D. Ukachi, M.O. Idris, O.T. Olaoba, I.O. Adedotun, O.E. Kolawole, Y. Xiaoxing, M. Abdul-Hammed, Molecular modeling in drug discovery, Inform. Med. Unlocked 29 (2022) 100880, https://doi.org/10.1016/j.imu.2022.100880.
[41] Z. Yang, W. Wang, Y. Qi, Y. Yang, C.-H. Chen, J.-Z. Liu, G.-X. Chu, G.-H. Bao, Exploring new catechin derivatives as SARS-CoV-2 Mpro inhibitors from tea by molecular networking, surface plasma resonance, enzyme inhibition, induced fit docking, and metadynamics simulations, Comput. Biol. Med. 151 (2022) 106288, https://doi.org/10.1016/j.compbiomed.2022.106288.
[42] H. Nada, K. Lee, L. Gotina, A.N. Pae, A. Elkamhawy, Identification of novel discoidin domain receptor 1 (DDR1) inhibitors using E-pharmacophore modeling, structure-based virtual screening, molecular dynamics simulation and MM-GBSA approaches, Comput. Biol. Med. 142 (2022) 105217, https://doi.org/10.1016/j.compbiomed.2022.105217.
[43] I. Mamedov, H. Şenol, F. Naghiyev, V. Khrustalev, N. Sadeghian, P. Taslimi, New tetrahydro-isoquinoline derivatives as cholinesterase and α-glycosidase inhibitors: synthesis, characterization, molecular docking & dynamics, ADME prediction, in vitro cytotoxicity and enzyme inhibition studies, J. Mol. Liq. 404 (2024) 125006, https://doi.org/10.1016/j.molliq.2024.125006.
[44] F.S. Tokalı, H. Şenol, Ş. Ateşoğlu, F. Akbaş, A series of quinazolin-4(3H)-one-morpholine hybrids as anti-lung-cancer agents: synthesis, molecular docking, molecular dynamics, ADME prediction and biological activity studies, Chem. Biol. Drug Des. 104 (1) (2024) e14599, https://doi.org/10.1111/cbdd.14599.
[45] M. Karplus, J.A. McCammon, Molecular dynamics simulations of biomolecules, Nat. Struct. Biol. 9 (9) (2002) 646–652, https://doi.org/10.1038/nsb0902-646.
[46] S.A. Hollingsworth, R.O. Dror, Molecular dynamics simulation for all, NeuronNeuron 99 (6) (2018) 1129–1143, https://doi.org/10.1016/j.neuron.2018.08.011.
[47] A. Verma, D.K. Waiker, N. Singh, A. Singh, P. Saraf, B. Bhardwaj, P. Kumar, S. Krishnamurthy, S. Srikrishna, S.K. Shrivastava, Lead optimization based design, synthesis, and pharmacological evaluation of quinazoline derivatives as multi-targeting agents for Alzheimer's disease treatment, Eur. J. Med. Chem. 271 (2024) 116450, https://doi.org/10.1016/j.ejmech.2024.116450.
[48] S. Zareei, M. Mohammadi-Khanaposhtani, M. Shahali, H. Şenol, M. Badbedast, A. Moazzam, S. Mohseni, E.N. Esfahani, S.F. Ekti, B. Larijani, M. Mahdavi, E. H. Ibrahim, H.A. Ghramh, P. Taslimi, Phenyldiazenyl-phenoxy-1,2,3-triazol-acetamide derivatives as new dual cholinesterase Inhibitors: design, synthesis, in vitro, and in silico enzymatic inhibition evaluations, J. Mol. Struct. (2024) 139686, https://doi.org/10.1016/j.molstruc.2024.139686.
[49] B. Zengin Kurt, D. Öztürk Civelek, E.B. Çakmak, Y. Kolcuoğlu, H. Şenol, B.N. Sağlık Özkan, A. Dag, K. Benkli, Synthesis of sorafenib−ruthenium complexes, investigation of biological activities and applications in drug delivery systems as an anticancer agent, J. Med. Chem. 67 (6) (2024) 4463–4482, https://doi.org/10.1021/acs.jmedchem.3c01115.
[50] L. Shi, Z. Wen, Y. Song, J. Wang, D. Yu, Computational investigation of potent inhibitors against SARS-CoV-2 2′-O-methyltransferase (nsp16): structure-based pharmacophore modeling, molecular docking, molecular dynamics simulations and binding free energy calculations, J. Mol. Graph. 117 (2022) 108306, https://doi.org/10.1016/j.jmgm.2022.108306.
[51] F.S. Tokalı, P. Taslimi, M. Sadeghi, H. Şenol, Synthesis and evaluation of quinazolin-4(3H)-one derivatives as multitarget metabolic enzyme inhibitors: a biochemistry-oriented drug design, ChemistrySelect 8 (25) (2023) e202301158, https://doi.org/10.1002/slct.202301158.
[52] H. Şenol, F. Çakır, 3-Amino-thiophene-2-carbohydrazide derivatives as anti colon cancer agents: synthesis, characterization, in-silico and in-vitro biological activity studies, ChemistrySelect 8 (39) (2023) e202302448, https://doi.org/10.1002/slct.202302448.
[53] Ö. Demirkıran, E. Erol, H. Şenol, İ.M. Kesdi, G.Ö. Alim Toraman, E.Ş. Okudan, G. Topcu, Cytotoxic meroterpenoids from brown alga Stypopodium schimperi (Kützing) Verlaque & Boudouresque with comprehensive molecular docking & dynamics and ADME studies, Process Biochem. 136 (2024) 90–108, https://doi.org/10.1016/j.procbio.2023.11.029.